Bi-monthly • November - December • 2017

ISSN: 0976-2108

BARC NEWSLETTER

Yellow rust resistant wheat variety DBW-88 developed by Gamma ray induced mutation breeding

Yellow rust infected wheat

CONTENTS

Non Contact Automated Inspection System for Wire Wrapped Fuel Elements

P.S. Somayajulu, K.V. Vrinda Devi, Rajashree Dixit, Prateek Pareek, Farman Ali and Madhusudan Sharma
Radiometallurgy Division
R. Rajakumar and B.N.Singh
FRFCF, Indira Gandhi Centre for Atomic Research, Kalpakkam
G.Sivasankaran
CWMF, Nuclear Recycle Board, Kalpakkam

The future cores of Prototype Fast Breeder Reactor (PFBR) fuel will be fabricated at the upcoming Fuel Fabrication Plant (FFP), Fuel Reactor Fuel Recycle Facility (FRFCF), Kalpakkam. The fuels pins are expected to be highly radiation hazardous owing to dirty plutonium. A fully automated metrology inspection system is developed which is compatible with high throughput rate of fabrication and eliminates radiation exposure to the personnel during metrology inspection. Complete metrology of the fuel pin is carried out in non contact manner using optical micrometers. The entire length of the pin is virtually divided into multiple segments and data from each segment is collected by scanning the pin with the micrometers in precisely controlled and indexed movements. All the specified dimensions are obtained by analyzing the full set of collected data ensuring good reliability in the results.

Introduction

The driver fuel of Prototype Fast Breeder Reactor (PFBR) is Uranium Plutonium Mixed Oxide ($(U,Pu)O_2$) MOX). MOX fuel pellets are loaded in SS-D9 clad tubes and hermetically sealed by welding end plugs at the ends[1].

The fuel pins are wrapped with D9 spacer wire to maintain element to element space in the reactor . The pin undergoes several steps of inspection to ensure weld integrity and conformance of other characteristics with the specifications. Metrological inspection is one of these quality control steps wherein the dimensions of the pin are ensured to be within the specified limits. The nominal dimensions of the fuel are shown in Table1.

Table 1: Nominal dimensions of PFBR fuel pin

Sl.No.	Dimension of fuel pin	Specification
1	Length	2580 ± 5 mm
2	Diameter (pin)	6.6 ± 0.02 mm
3	Diameter (wire)	1.6 ± 0.02 mm
4	Pitch	200 ± 5 mm
5	Bow	< 1 mm/ m

Metrological inspection of finished fuel pins involves precise measurement of various details such as pin length, pin diameter, pitch of spacer wire wrapping, gap between the wrapped wire and the pin, bow etc. to ensure their conformances with the specifications. Though individual structural components are checked meteorologically for their acceptance, it is very important to ascertain the correctness of the dimensions in the finished fuel pin due to various processes and handling involved which can cause certain dimensional changes. Deviations from the specifications may have serious consequences on the in-reactor behavior of the fuel pin and can be aggravated and lead to failures[2,3]. Additionally, any deviations from these characteristics pose difficulties during configuration of fuel sub-assembly or clusters. These variations can result in development of undesired stresses on the fuel pin and also on adjacent pins during irradiation.

As the fuel contains radioactive nuclides, contact inspection results in considerable man-rem to the operator which can be avoided by incorporating automated systems. The inspection

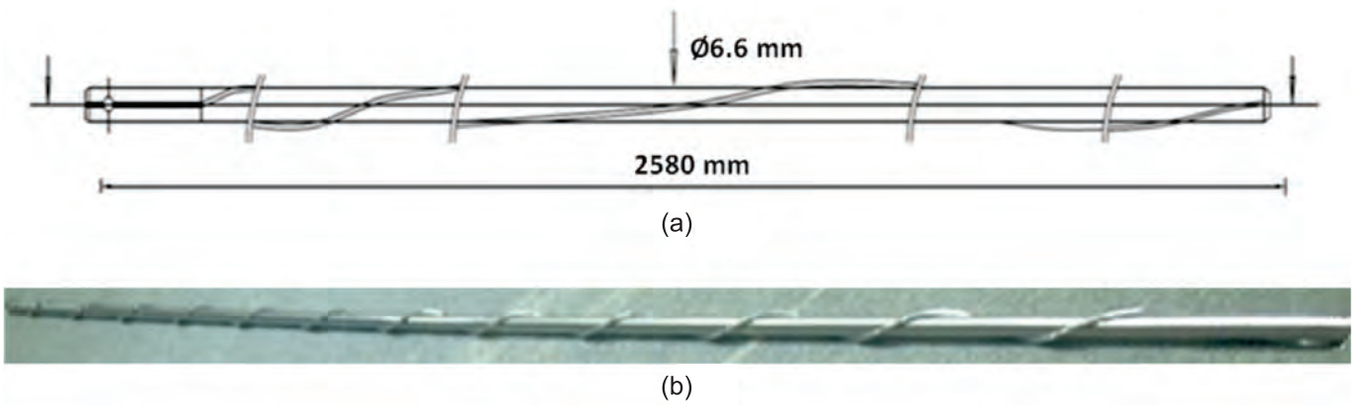

Fig.1: (a): Schematic of PFBR fuel pin (b): Actual photograph of the pin

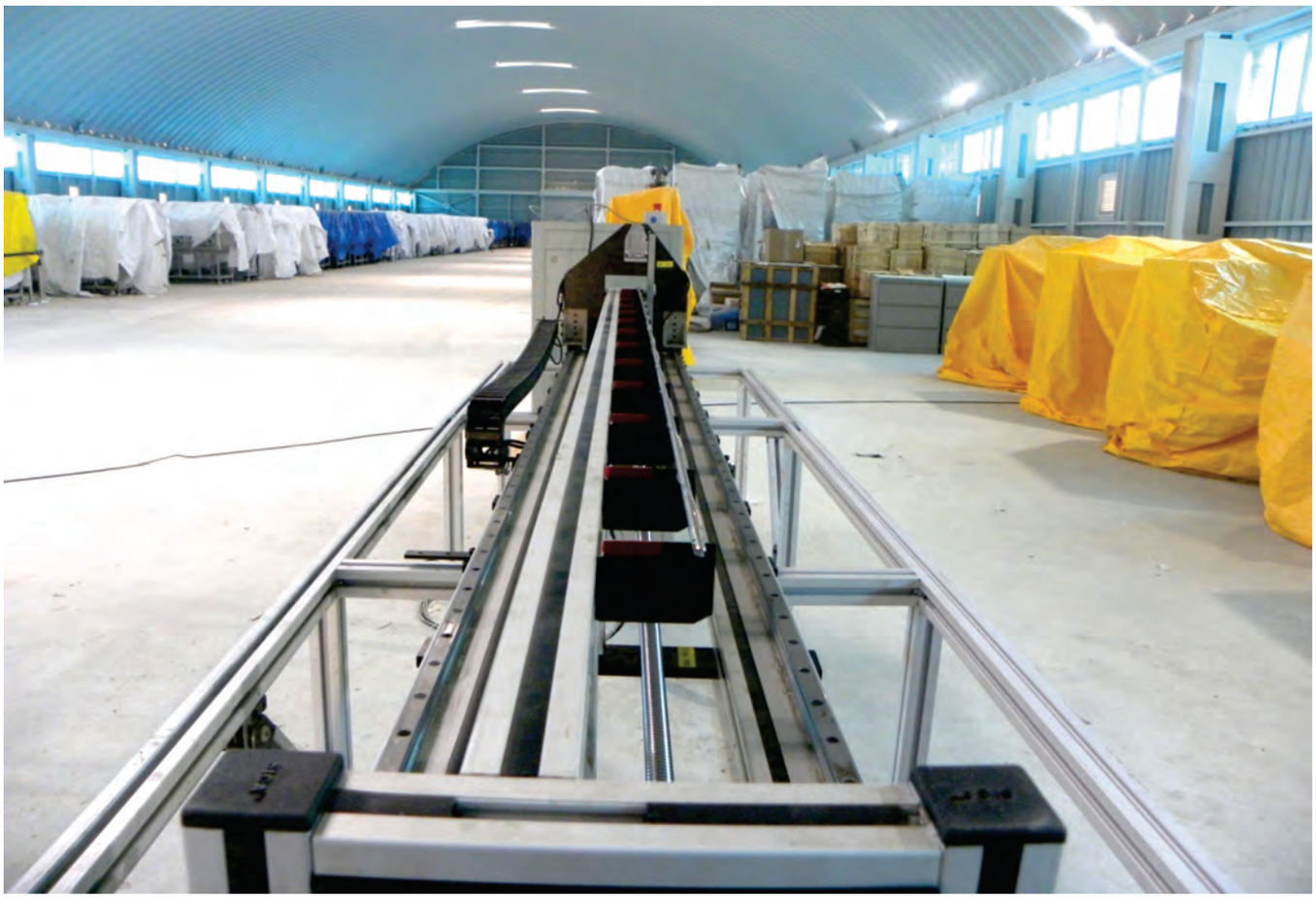

Fig. 2: Actual photograph of Bow measurement system

system being noncontact and automated helps in damage free handling during inspection while matching with the production rate of high throughput fuel fabrication facilities.

A fully automated non-contact measurement system has been developed for metrological inspection of PFBR fuel pins. Fig. 1(a) and 1(b) show the schematic and actual photograph of PFBR fuel pins respectively.

The system consists of two optical micrometers placed perpendicular to each other which scan the fuel pins over the length in controlled and indexed movement. During this operation the probing light beam gets intersected by the pin and the analyses based on the output beam provide the required details for the pin metrology. The system is highly versatile and is completely free of pre-positioning of the pins thereby minimizing human intervention. The cycle time of the system for a fuel pin of length ~2580 mm is approximately 18 minutes. The system is not specific to PFBR fuel pins and is capable of inspecting any pin up to a length of 2700 mm. Photograph of the system is shown in Fig.2.

Methodology

An optical micrometer performs non-contact measurements on any object which intercepts it. It performs in line measurement with high speed and precision. The optical micrometer used in the system is based on Gallium Nitride high intensity LED having a measuring range of 0.3-35 mm. The high intensity of the emitted light eliminates interference from stray light in the sensor. A linear array of CCD detectors is placed in front of the transmitter which senses the dimensions of the object that intercepts the light with ±2 μm accuracy. The principle of measurement was based on the variation in the interception of the incident light beam by the object as illustrated in Fig.3 length of the pin, diameter of the pin and the wire, pitch of wire wrapping, gap (if any) between the wrapped wire and pin and bow of the fuel pin can be measured using this system. The light beam is intercepted by the pin perpendicular to the axial direction. The system is indexed at every 5 mm and information is mapped as per data collected at these intervals.

The light beam is intercepted only by the pin at certain locations and by the pin along with the wire at certain other locations as shown in Fig 4. The outgoing light will be split into multiple segments depending on the intercepting condition of the pin and the wire. The detector receives

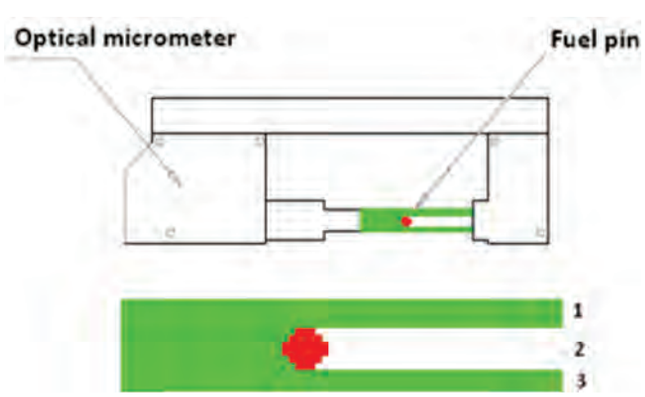

Fig. 3: Interception of a fuel pin using optical micrometer

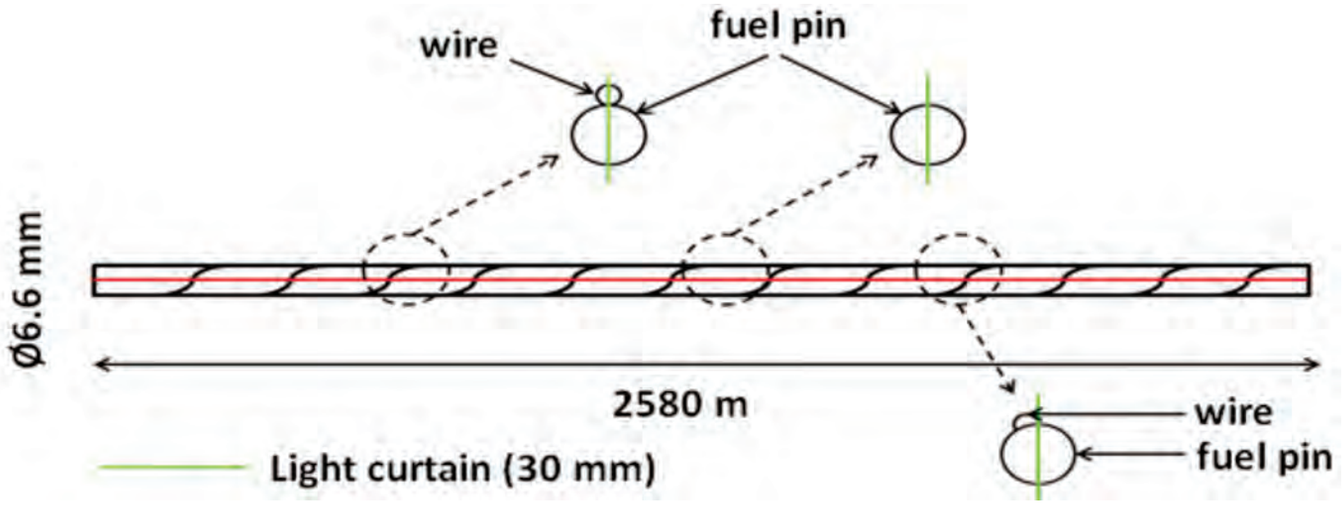

Fig. 4: Light beam intercepting at various locations of pin.

distinct light segments i.e. E12, E13, E14 etc. after interception as shown in Fig.5 and the system acquires these indexed data over the length of the pin at every 5mm interval. The system is capable of measuring all the individual segments, however to simplify the computation and optimize the results and run time E12 and E13 are only considered. The system analyses the variation between the maximum and minimum of each segment which in turn corresponds to the interception of light as in three different cases viz; by the pin alone or by the pin along with the wire or by the pin and wire with a gap in between. The system also uses pre-fed data (pin dimensions, wire diameter and wrapping pitch) in a comparator logic used by the software which supports in differentiating the three possible cases of interceptions.

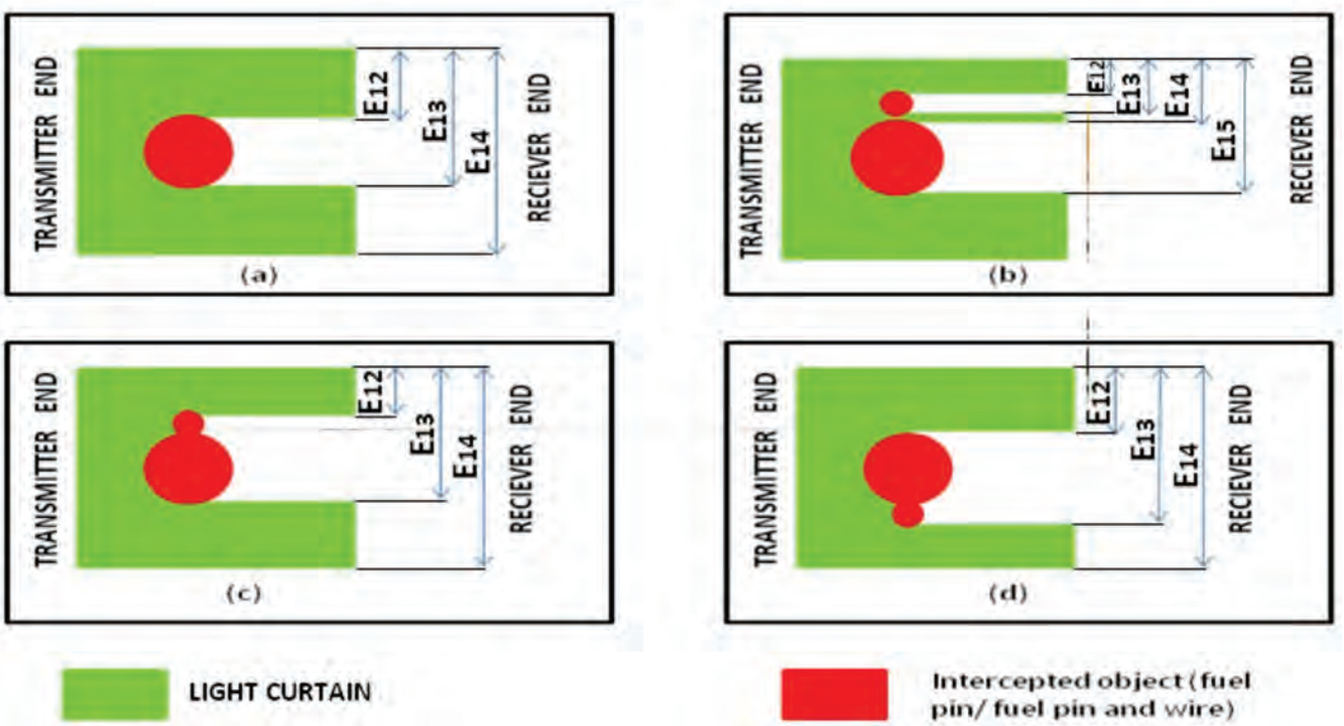

Fig. 5: (a) Light beam intercepting with the fuel pin. (b) Light beam intercepting with the fuel pin along with the wire having a gap between them. (c) Light beam intercepting with the fuel pin along with the wire on the top. (d) Light beam intercepting with the fuel pin along with the wire on the bottom.

Table 2: Logical analysis of different cases of light interception

Case	Segment E12	Segment E13	Interception with light curtain	Measurable dimension using comparative logic
1	Maximum	Maximum	Pin with wire at the bottom.	Wire diameter, pitch & bow
2	Maximum	Minimum	Pin without wire.	Pin diameter
3	Minimum	Maximum	Pin with wire at the top.	Wire diameter, pitch & bow

The number of portions into which the light beam is divided (four in case of a gap and three otherwise) will be able to indicate whether there is any gap between the spacer wire and the pin as illustrated in Fig.5. The value of E13 is also analyzed with the help of the pre fed data to confirm the occurrence of any gap between the pin and the wire. If E13 is exceptionally low (referred to the pre fed data), a gap is understood to be present. If not, it is assumed that there is no gap present between the wire and the pin. In any case, if a gap exists, the pin has to be rejected and the scanning stops generating an alarm.

Assuming non existence of any gap further measurements is carried out with the following logic. The variation of E12 and E13 will indicate the positions of the wire around the pin. The different logical cases for measurement are as explained in Table 2.

Length measurement is carried out using end point detection and precise control of encoder positioning by using a ball screw in the axial direction of the pin. The pin shall be placed roughly within the marked region on the scanning table. A fine indexing at 1mm interval is performed to accurately detect the start point of the pin during the first 20 mm of scanning. Then the micrometers are indexed at every 5 mm interval till it reaches the last 20 mm of the stroke length which is again scanned with fine indexing of 1mm to identify the end point of the pin accurately. The difference between the readings corresponding to the two end points of the fuel pin gives the length of the pin. Diameters of the pin obtained from the difference of E12 and E13 at positions of interception where case 2 of Table 2 is applicable. Average pin diameter is subtracted from the difference of segments E13 and E12 in cases 1 and 3 of Table 2 to obtain the wire diameter.

Pitch of the wire wrap is measured by calculating the average axial distance between two consecutive wrappings. Case 1 and case 3 of Table 2 are considered for measurement of half pitch. Difference of the encoder positions corresponding to the maximum value of segments E13 and E12 are registered over the length of the pin. Double of the average of these values will be measured as the pitch of the spacer wire wrap.

The principle of bow measurement which is illustrated in Fig. 6 is as follows. Two identical micrometers shall be used which are placed mutually perpendicular to the pin axis. The pin is divided into three segments, i.e. two segments of 1 meter each and the last segment of the rest of the length, as shown in the figure. For each segment the bow along the horizontal axis will be measured by a micrometer mounted in such a way that the light beam incident on the pin parallel to Z-axis (vertical direction). The tube will be placed on multiple cantilever support points. The segment E12 will show consistent values if the pin is straight and placed parallel to the light beam. If the pin is having bow, the values of E12 will go on increasing till it reaches a peak value and then it will show a reverse trend. The ideal center line (with no bow) of the tube will be simulated by joining the centre points of the end cross sections of each segment by a straight line. The real central line of the pin is obtained by joining the centre points of each cross section of the tube intercepting the light beam in each segment. The maximum deviation of the real centre line from the ideal one depicts the value of bow on the pin in each segment. Overall bow of the pin is obtained by drawing the ideal and actual centerline of the entire pin and measuring the deviation. The same procedure is simultaneously carried out by another micrometer mounted in horizontal direction for measurement of bow in the vertical direction also. Thus, the system is capable of giving bow at each segment as well as the whole pin in XY and YZ planes.

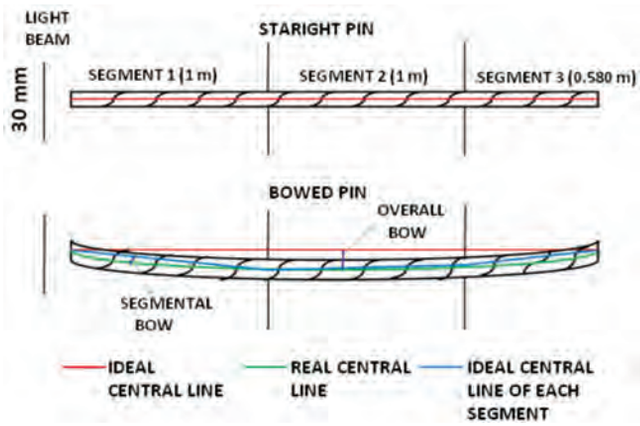

Fig. 6: Principle of Bow analysis

System Description

The mechanical part of the system includes a scanning table, two mutually perpendicular assemblies of optical micrometer, ball screw for the axial movement of the micrometer assemblies, encoder to index the scanning and the cantilever supports for pin as shown in Fig.7(a). A photograph of the actual system is given in Fig. 7(b). The ball screw with 5 mm pitch and 20 mm diameter has a travel of 2700mm on X-axis and 10μm resolution. Ball screw is driven by servo motor of 400W rating and 2000 rpm.

The entire system is controlled using a PC based motion controller with appropriate software for implementing the movement for scanning, data capture from the micrometer controller, off line data analysis and reporting. Communication with the PC is through Ethernet cable.

Optical micrometer assembly acquires the home position automatically prior to every scan irrespective of the position of the pin. This ensures independence of measurements from the pin position and orientation. On receipt of start command from the PC, the micrometer assemblies start moving with the help of the ball screw. This movement is precisely indexed over the entire stroke length by means of position feedback from the encoder.

As the optical beam gets intercepted by the pin, the light curtain is divided into multiple segments which are detected by the detector. The lengths of the segments are recorded at

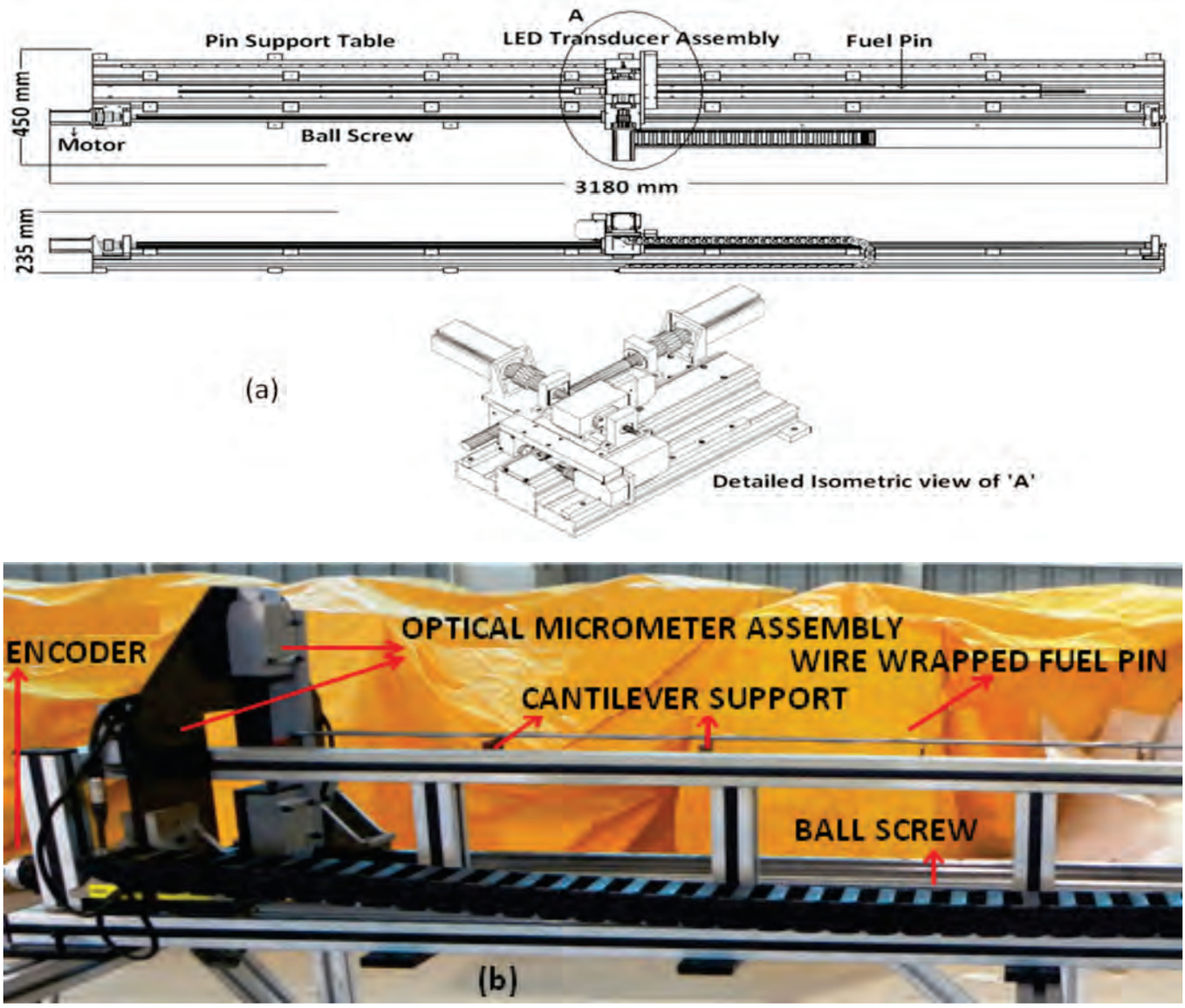

Fig.7 (a): General arrangement drawing of the system (b) Photograph of the actual system

every 5 mm of the stroke length and the data is analyzed to obtain the required dimensions as explained in earlier section. A customized software application was developed in Matlab to analyze the data which provides a graphical output of the complete profile of the fuel pin along with all the necessary dimensional values. The graphical output enables the operator to select and inspect any specific region of interest if needed in detail. The software is also capable of generating a detailed tabular report based on raw data.

Results

The graphical representations as well as the tabular reports are simultaneously provided by the system as shown in Fig.8. The report obtained shows graphical representation on the left side and the measurements are given in tabular form on the right side. The graphs corresponding to the scanning along the horizontal and vertical planes are shown separately in the report. The segments E12 and E13 [Fig.6] are analyzed to identify the interception points at every 5 mm interval. The value of E12 and E13 are plotted against the encoder readings to generate the graphical representation of the wire wrapped fuel pin. The upper part of the green and red coloured portions in the graph is obtained from the values of E12 and the corresponding lower part from E13. The central white line is computed from the values of E12 and E13. The graphical representation equips the operator with better judgement of the pin dimensions.

The average, minimum and maximum diameter of the pin is displayed on the first row of the tabular report. The second row indicates the encoder readings corresponding to the first and the last positions of the micrometer where the light curtain is intercepted by the fuel pin. The difference of these two readings will be measured as the length of the pin which is displayed in the third box of the second row. Average pitch of the wire wrap along with the deviation over the pin length is displayed in row three. Average diameter of the wire is displayed in the fourth row along with its deviation.

There are two tables in the fifth row which display the bow values measured along the horizontal and vertical planes. Each table has four rows which show the values of the maximum bow in each segment along with its position

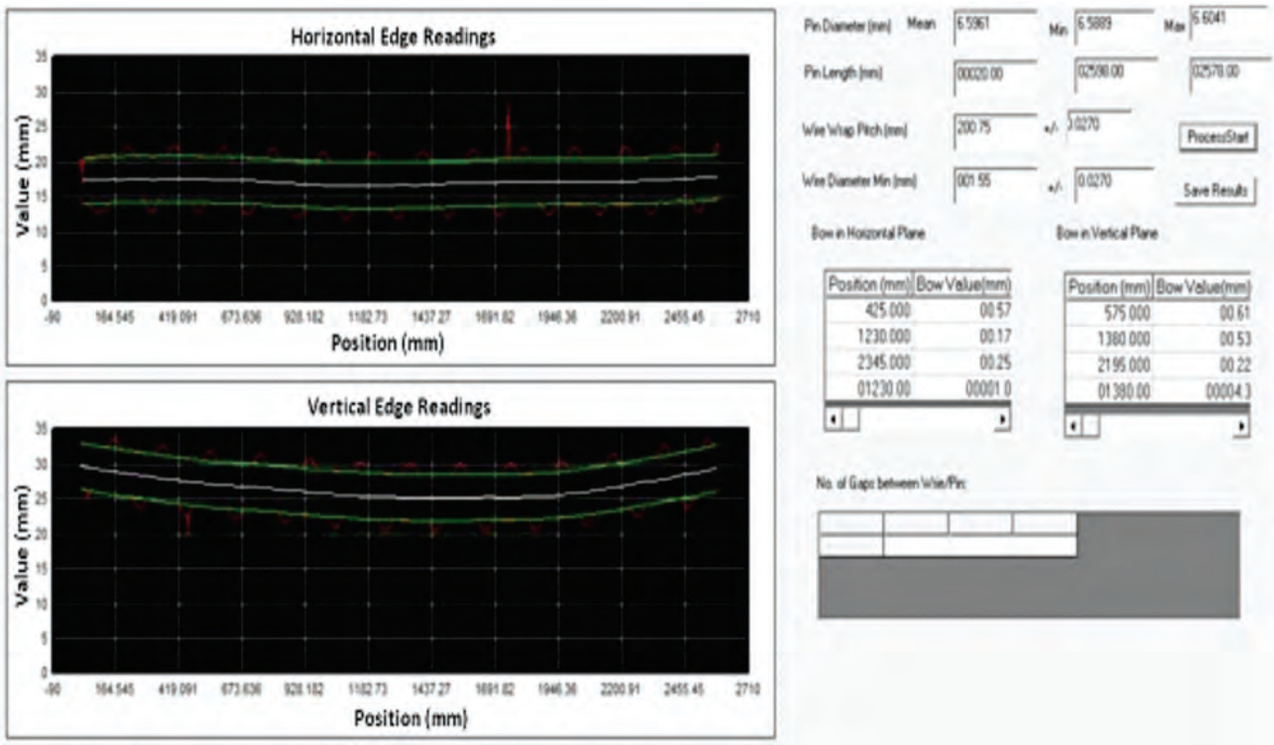

Fig.8. Screen shot of the system report

followed by the maximum bow over the entire length and its position [Fig.6]. The next row indicates the positions corresponding to the gaps between the wire and the pin if any detected.

The system has been tested and multiple trials were conducted using a wire wrapped pin by changing its orientation and positioning. The repeatability of the system for the measurement of length, pin diameter, wire diameter, pitch and bow obtained during these trials was found to be ±10 μm, ±20 μm, ±20 μm, ±200 μm and ±200 μm respectively.

Conclusion

A fully automated metrology inspection system for PFBR fuel pins developed offers the following features and benefits:

- Complete metrological inspection of the pin in a single scan with zero manual intervention.
- Offers flexibility of measuring fuel pins of any configuration within the scanning length of 2700 mm.
- Auto-homing of optical micrometer assembly ensuring precise measurements irrespective of the orientation of the pin.
- Zero operator intervention due to independence of measurements from pre-positioning of the pin.
- Highly reliable results due generation of large measurement data from very high scanning points (every 5 mm interval). The indexing value of 5 mm was chosen for optimization of scanning time and reliability of the results. The system completes metrology of a PFBR pin in 18 minutes.
- Precise variation of every dimension over the length of the pin is also obtained along with the average values.
- Detailed analysis of bow (segmental and overall) obtained in single scan.
- Graphical representation of complete pin is constructed and obtained along with the pin dimensional measurements for operator decision.
- The system is designed to be rugged, low on maintenance and suitable for continuous operation for high throughput of pins.
- System is amenable to further reduction in scanning time by adapting customised algorithms depending on the pin configuration and specified requirements.

Acknowledgement

The authors sincerely express their gratitude to Shri Vivek Bhasin, Head, RMD and A.D, NFG for his valuable support. We would also like to express our thanks to Shri P. Kumarsekaran, Shri Prashant Kumar Singh and Shri S. Meenatchi Sundaram of FRFCF, Kalpakkam for their contribution in conducting the trials. The support extended by Shri S. Chakraborty, Dr. Anupam Saraswat and Shri A.K. Mishra is gratefully acknowledged.

References

1. Recycle Fuel Fabrication for Closed Fuel Cycle in India, H.S. Kamath, Energy Procedia 7 (2011) 110–119.
2. Interactions Between Fuel Pins And Assembly Components, D.O. Pickman, Nuclear Engineering and Design 33 (1975) 125-140.
3. Fuel pin bowing in CAGR, I.G. Crossland, International Nuclear Information System (INIS) 1982-01-01.

Cost-Effective In-house Synthesis of Peptides for Preparation of Peptide-Based Cancer-Specific Radiopharmaceuticals

Drishty Satpati, Ashutosh Dash
Radiopharmaceuticals Division

Peptides are the molecules having high affinity towards receptors expressed in high density on tumor cells. High specificity and small size of peptides allows for rapid and selective localization in the tumor leading to high tumor-to-background contrast during imaging. Receptor-targeted radiolabeled peptides thus hold great promise in oncology for clinical diagnosis and targeted radionuclide therapy. However the high cost of peptide and dependence on commercial suppliers decreases their affordability and accessibility for a larger population. Cost-effective in-house synthesis of peptides and development of freeze-dried kits thereof for preparation of cancer-specific radiopharmaceuticals is an economically viable alternative. Indigenously synthesized peptides shall boost the availability of peptide-based radiopharmaceuticals to larger masses. Hence, solid phase peptide synthesis facility set-up at Radiopharmaceuticals Division has been utilized for indigenous synthesis of DOTA-TATE, a peptide widely used in nuclear medicine hospitals for PET imaging (^{68}Ga-DOTA-TATE) and radiotherapy (^{177}Lu-DOTA-TATE) of patients suffering from neuroendocrine tumors.

Introduction

Development of cancer-specific radiopharmaceuticals is a challenging job as the molecules chosen for this purpose should be capable of distinguishing between cancerous regions and normal tissues so as to limit the off-target toxicity. The cancer cells can be discriminated from normal cells on the basis of altered cell metabolism, proliferation, angiogenesis, hypoxia and apoptosis as well as change in levels of receptors, enzymes or hormones. These processes can be targeted by employing radiolabeled small molecules/ peptides/ antibodies as cancer-specific radiopharmaceuticals for imaging and therapy. High affinity and specificity towards the target (high tumor uptake and retention), rapid clearance from non-target organs and *in vivo* stability are the criteria for acceptability of these probes for *in vivo* applications [1].

Peptides having high specificity towards their target and low toxicity are the most promising probes for molecular imaging and therapy of different cancers. Peptides are short chain of amino acids linked by peptide bond (-CO-NH) and are discriminated from larger antibodies on the basis of molecular weight (1-2 kDa) and number of amino acids (<50) (Fig. 1). Peptides having size intermediate to that of small molecules (<1 kDa) and antibodies (~150 kDa) demonstrate more favorable biodistribution profile (higher tumor permeability, rapid blood clearance) [2]. Besides, ease of synthesis and modification, absence of any immunological response or toxic metabolic products highlight the profound potential of peptides as cancer-seeking probes. The major problem encountered during the use of peptides is *in vivo* enzymatic degradation or rapid kidney clearance which can be prevented by incorporation of D-amino acids/cyclization or introduction of polyethylene glycol (PEG) moiety respectively. Peptide ligands can be readily and reproducibly constructed by solid phase peptide synthesis (SPPS) and also modified to optimize their binding affinity, improve stability against proteolytic degradation and increase *in vivo* half-life. Peptide ligands exhibit high affinity and specificity towards receptors over-expressed in cancer cells. These peptide-binding receptors are present in high density in tumors in comparison to normal cells thus making them potential targets for detection, staging and therapy with specifically designed peptide-based radiopharmaceuticals. Somatostatin receptor (SSTr) over-expression in neuroendocrine tumors has been well exploited for development of radiolabeled somatostatin peptide analogs which are highly used in nuclear medicine clinics for molecular imaging and therapy of NETs. Octreotide is a cyclic octapeptide consisting of 8 amino acids from somatostatin [D-Phe^1-Cys^2-Phe^3-D-Trp^4-Lys^5-Thr^6-Cys^7-Thr^8-ol] that specifically target somatostatin receptors [3]. This peptide has set a paradigm for the development of other tumor specific peptides.

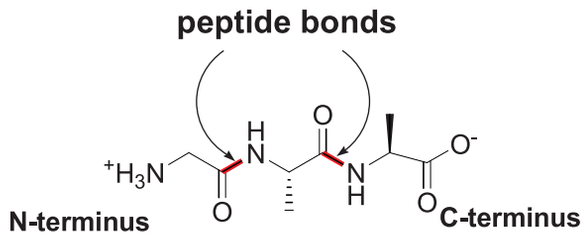

Fig. 1: Structure of a peptide bond

Peptide-based radiopharmaceuticals targeting specific disease processes in particular tumor growth and metastasis facilitate cancer diagnosis and treatment as well as monitoring of therapeutic response. However peptides procured from commercial suppliers are exorbitantly priced escalating the cost of peptide-based radiopharmaceuticals which is ultimately borne by cancer patients. These peptides if synthesized indigenously shall reduce the cost of radiopharmaceuticals and thus ease the financial burden on patients.

Peptide Synthesis

Robert Bruce Merrifield first introduced the concept of solid phase peptide synthesis (SPPS) allowing the rapid assembly of a peptide chain through successive reactions of amino acids onto an insoluble porous support. Solid phase peptide synthesis is a quick and easy approach requiring fewer purifications in comparison to solution phase synthesis and leading to high yields. SPPS employs large excess of reagents at high concentration to drive coupling reactions to completion. After the reaction, excess reagents and side products are washed off by filtration and thus do not interfere in subsequent steps that are performed in the same reaction vessel.

The solid support consists of small, polymeric 'resin' beads functionalized with reactive 'linker' groups (such as amine or hydroxyl groups) onto which peptide chains are built. The peptide remains covalently attached to the support throughout the synthesis, allowing it to be easily isolated from reagents and reaction by-products after each step via simple filtration and washing of the polymer beads with a solvent (DMF). N-terminus and side chains of amino acids are protected by groups like Boc, Fmoc etc. to avoid unwanted reaction at those groups during the peptide coupling step [4].

Peptides were synthesized manually in our laboratory by SPPS using Fmoc (fluorenylmethoxy carbonyl) strategy where N-terminus of amino acids was protected by Fmoc group which can be easily removed by a mild base (20% piperidine in DMF). Peptide then can be finally cleaved from the solid support using trifluoroacetic acid (TFA) and purified by semi-preparative HPLC.

The modified octreotide analog [Tyr^3,Thr^8] octreotide commonly known as TATE needed for preparation of diagnostic radiopharmaceutical, ^{68}Ga-DOTA-TATE and therapeutic radiopharmaceutical, ^{177}Lu-DOTA-TATE has been synthesized in-house as a cost-effective alternative to expensive commercial peptide.

DOTA-TATE

Radiolabeled somatostatin peptide analogs (octreotide, octreotate) are the most successful peptide-based radiopharmaceuticals for targeted imaging and therapy of neuroendocrine tumors (NETs) expressing somatostain receptors (sstr's). Ga-68-labeled somatostatin analog, [^{68}Ga]DOTA^0-Tyr^3-octreotate, [^{68}Ga]DOTA-TATE is a clinically established accurate standard for PET imaging of neuroendocrine tumors [5]. The availability of peptide may be sometimes restricted by patents, by the cost or by the limitation in the number of suppliers. Since [^{68}Ga]DOTA-TATE is the gold standard for NET imaging, delay in the supply of the DOTA-TATE peptide can be detrimental for NET patients. The in-house sourcing of the peptide for radiolabeling with ^{68}Ga can provide an easily accessible and economically viable solution.

The peptide DOTA-TATE was synthesized indigenously by solid phase peptide synthesis using standard Fmoc strategy. The chemical structure of DOTA-TATE is presented in Fig. 2A. The crude peptide was purified by semi-preparative HPLC and characterized by mass spectroscopy. MS: m/z observed = 1433.7, $[M+2H]^{2+}$ 717.7 calculated = 1434.6; Analytical HPLC (220 nm): >97 % purity.

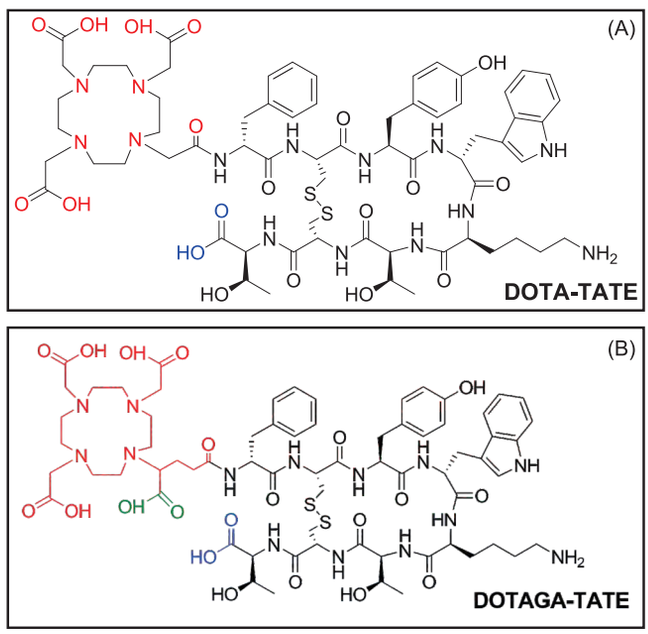

Fig. 2: Chemical structure of (A) DOTA-TATE and (B) DOTAGA-TATE

In-house synthesized DOTA-TATE was radiolabeled with $^{68}GaCl_3$ in high radiochemical yield and purity (>98%) and HPLC chromatogram (peak and retention time) was compared with the commercially obtained peptide (Fig. 3A and 3B) where good concordance was observed.

Single vial freeze-dried kits containing in-house synthesized DOTA-TATE peptide (50 µg) were developed which can be used for preparation of 4-5 patient doses in a hospital setting. Biodistribution studies of kit-formulated ^{68}Ga-DOTA-TATE were conducted in normal Swiss mice where rapid clearance from blood and other non-target organs was observed. The clinical validity of kits was established by performing PET/CT imaging studies at KMCH (Kovai Medical Center and Hospital, Coimbatore). Kits were tested with 2 mL of $^{68}GaCl_3$ (888 MBq, 24 mCi) eluted from ITG generator at the hospital. The vial was incubated at 90°C for 5-10 minutes. Radiochemical yield was >98% as determined by instant thin layer chromatography-silica gel paper (ITLC-SG).

^{68}Ga-DOTA-TATE PET/CT imaging in patients with well differentiated NET's indicated high tumor to background ratio and even low volume metastasis to skeleton and lungs was picked up by ^{68}Ga-DOTA-TATE (Fig. 4 A).

DOTAGA-TATE

The macrocyclic chelator DOTA is suitable for complexation with diagnostic (^{68}Ga) as well as therapeutic radiometals (^{177}Lu) and thus has wide applicability in preparation of radiopharmaceuticals. The newer promising variant of

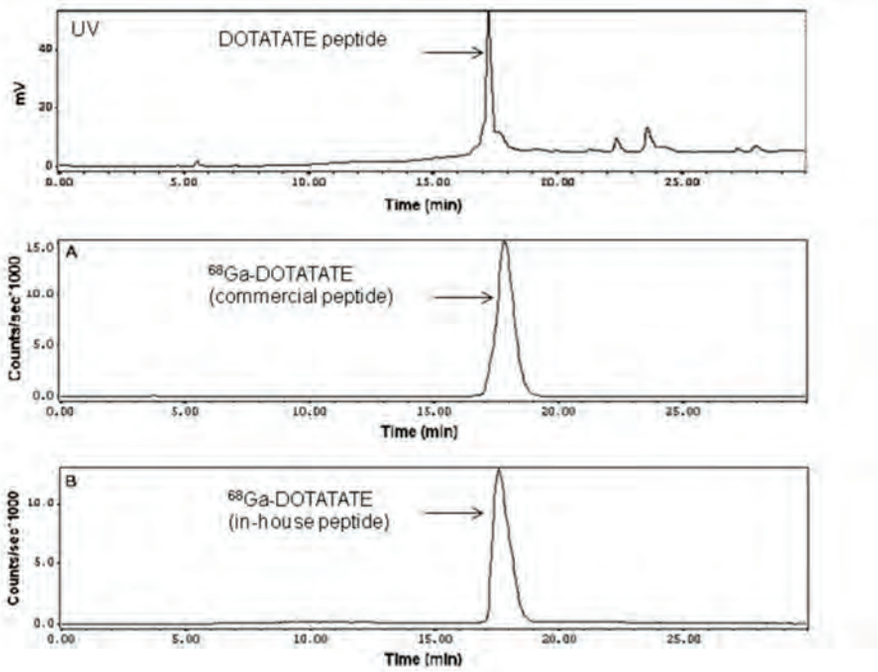

Fig. 3: UV-HPLC chromatogram of synthesized DOTA-TATE peptide; Radio-HPLC chromatogram of ^{68}Ga-DOTA-TATE (A) prepared from commercial peptide, (B) prepared from in-house synthesized peptide

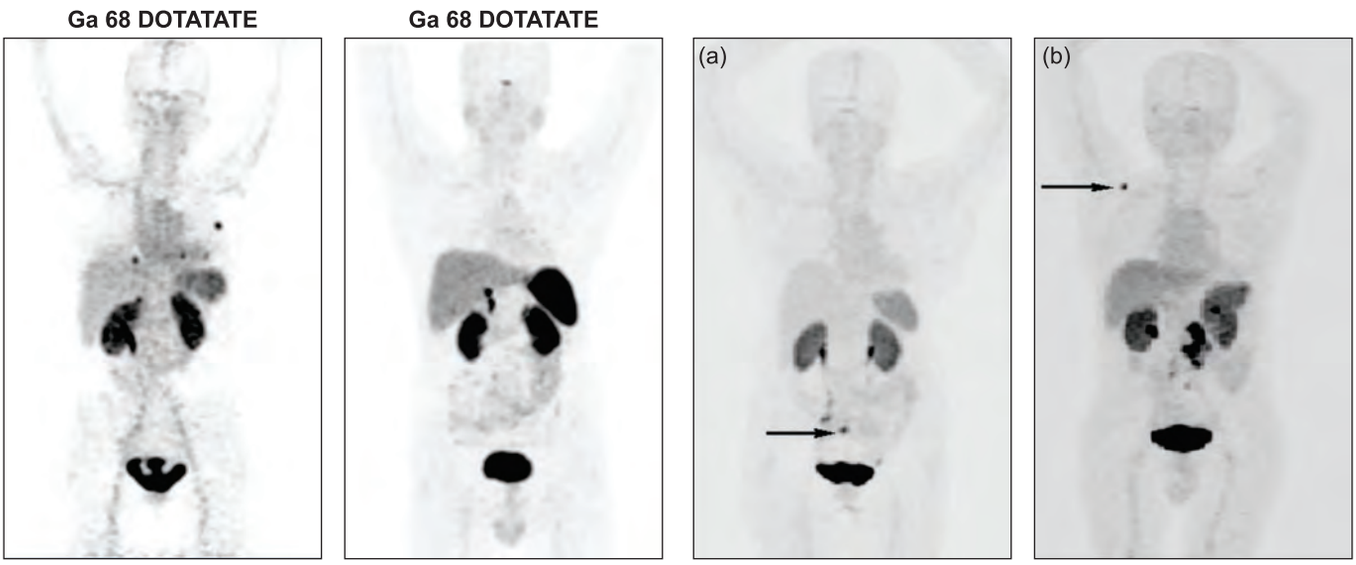

Fig. 4: PET/CT images of (A) ^{68}Ga-DOTA-TATE and (B) ^{68}Ga-DOTAGA-TATE in patients suffering from neuroendocrine tumors

DOTA with five carboxyl groups is 1,4,7,10-tetraazacyclododecane,1-(glutaric acid)-4,7,10-triacetic acid (DOTAGA) [6]. The extra carboxyl group of DOTAGA imparts higher hydrophilicity to complexes compared to DOTA. Of the four carboxyl groups present in DOTA one is utilized for conjugation with the peptide hence it forms neutral complexes with trivalent metal ions ($^{68}Ga^{3+}$/ $^{177}Lu^{3+}$ / $^{90}Y^{3+}$) whereas DOTAGA having four carboxyl groups left after peptide conjugation leads to formation of negatively charged complexes with these ions.

The conjugate DOTAGA-TATE (Fig. 2B) was synthesized by solid phase peptide synthesis in a similar manner as DOTA-TATE. The crude peptide was purified by semi-preparative HPLC and characterized by mass spectroscopy. MALDI-TOF MS: m/z 1506.6 observed (calcd for $C_{68}H_{94}N_{14}O_{21}S_2$: 1507.6).

Single vial freeze-dried kits containing in-house synthesized DOTAGA-TATE peptide (50 µg) were developed for preparation of 4-5 patient doses in a hospital setting. Biodistribution studies of ^{68}Ga-DOTAGA-TATE were conducted in normal Wistar rats and compared with ^{68}Ga-DOTA-TATE. [^{68}Ga]DOTAGA-TATE exhibited almost similar blood clearance to that reported for [^{68}Ga]DOTA-TATE. However significantly ($p<0.05$) fast clearance from the intestine, spleen, stomach, lungs and heart was observed for [^{68}Ga]DOTAGA-TATE compared to [^{68}Ga]DOTA-TATE.

DOTAGA-TATE kits were clinically evaluated on formulation with ^{68}Ga eluted from ^{68}Ge/^{68}Ga generator [ITG, Germany (0.05 N HCl)] at KMCH (Kovai Medical Center and Hospital, Coimbatore). Kits were tested with 2 mL of $^{68}GaCl_3$

(888 MBq, 24 mCi) and the high radiochemical yield (>98%) determined by instant thin layer chromatography-silica gel paper (ITLC-SG) indicated suitability of kits for preparation of 4-5 patient doses of 5 mCi each.

The omental metastasis in a 49-year-old female patient was clearly visible in [^{68}Ga]DOTAGA-TATE PET/CT scan and no other site of involvement was observed (Fig. 4B). In another patient, the pancreatic neuroendocrine tumor and the right scapular metastasis could be well identified by [^{68}Ga]DOTAGA-TATE. PET/CT images indicate that kit-formulated [^{68}Ga]DOTAGA-TATE could clearly identify sites of primary as well as metastatic disease with good accuracy and specificity.

Conclusions

Early detection of disease, personalized treatment and targeted therapy is the major aim of clinicians catering to cancer patients in nuclear medicine hospitals. The developing technology can benefit the general population if it is accessible to them at an affordable cost. The expensive peptides commercially procured lead to escalation of the cost of peptide-based radiopharmaceutical acting as a deterrent factor for patients to undergo diagnostic scans. In the present scenario with increasing incidences of cancers, in house synthesized peptides seem to be an economically viable option for reaching out the peptide-based radiopharmaceuticals to the larger volume of patients.

Acknowledgements

Authors acknowledge contribution of Dr. Anupam Mathur from BRIT for performing mass spectroscopy of peptides. Authors are also thankful to Dr. H. D. Sarma for performing biodistribution studies. Authors would also like to thank the clinical collaborator Dr. Ajit Shinto, Kovai Medical Centre and Hospital, Coimbatore for clinical evaluation of ^{68}Ga-labeled peptides.

References

1. Okarvi S. M. Peptide-based radiopharmaceuticals and cytotoxic conjugates: Potential tools against cancer. *Cancer Treat Rev*, 34, 2008, 13–26.
2. Fani M., Maecke H. R., Okarvi S. M. Radiolabeled peptides: valuable tools for the detection and treatment of cancer. *Theranostics,* 2(5), 2012, 481-501.
3. Wang L., Tang K., Zhang Q., Li H., Wen Z., Zhang H., Zhang H. Somatostatin receptor-based molecular imaging and therapy for neuroendocrine tumors.. *BioMed Res Int*, Article ID 102819, 2013, 1-11.
4. Amblard M., Fehrentz J. A., Martinez J., Subra G. Methods and protocols of modern solid phase peptide synthesis. *Mol Biotechnol,* 33, 2006, 239-254.
5. Ambrosini V., Campana D., Tomassetti P. Grassetto G, Rubello D, Fanti S. PET/CT with ^{68}Gallium-DOTA peptides in NET: an overview. *Eur J Radiol*, 80: 2011, e116–e119.
6. Westerlund K., Honarvar H., Norrström E. Strand J., Mitran B., Orlova A., Karlström A. E., Vladimir T. Increasing the net negative charge by replacement of DOTA chelator with DOTAGA improves the biodistribution of radiolabeled second-generation synthetic affibody molecules. *Mol Pharm,* 13, 2016, 1668–1678.

Development of Process for Decontamination of HEPA filter

C.K. Chakrabarti and K.M. Singh
FRWMD, Nuclear Recycle Board
S. Bhowmick and K.T. Shenoy
ChED, Chemical Engineering Group
S.K. Gupta
UED, Material Group

A significant volume of solid waste is generated from the exhausted High Efficiency Particulate Air (HEPA) filters in front and back end of fuel cycle facilities and operation of nuclear reactor. In the present work a treatment method has been explored to decontaminate the HEPA filter to such an extent so that subsequent volume reduction by compaction is possible and it can be directly disposed to RCC trenches (RCCT) with less spread of contamination. In a simulated experimental study fine particles of magnesium oxide (simulant of uranium oxide) were loaded into the filters to generate exhausted HEPA filters (200 mm × 170 mm × 150 mm) for trial runs. The leaching/ dislodging of particles from filter were investigated in an air – agitated leach vessel. With a series of trial runs, the methodology of filter decontamination has been improved and operating parameters were optimized. This experimental investigation provides practical inputs on design of the HEPA filter decontamination system.

Introduction

A substantial amount of High Efficiency Particulate Air (HEPA) filters are used in front and back end of fuel cycle facility and reactor operation for off gas treatment and ventilation system. Those filters are replaced based on the pressure drop or surface dose criteria. Hence, a substantial volume of solid waste is generated from the exhausted HEPA filters. Based on the activity content, this solid waste are also varied widely form Cat – I (D ≤ 0.2 R/ h) to Cat – III (D > 2 R/ h) and even alpha waste (i.e. Cat – IV, alpha activity > 4000 Bq/ g). In present practice, treatment for this type of solid waste is volume reduction by compaction for only non-alpha with low surface dose rate HEPA filters. High surface dose [Cat-II (0.2 < D ≤ 2) & III] non alpha HEPA filters are directly disposed (without any treatment) to RCC trenches (RCCT) or Tile holes (TH) of Near Surface Disposal Facility (NSDF) based on their surface dose criteria. Alpha contaminated solid waste (HEPA) also directly stored in the interim alpha storage facility without treatment. Hence in current scenario with increasing and expanding demand of fuel cycle facility proper treatment, conditioning and management of this type of solid waste is the utmost need for minimization of precious space of shallow land as well as deep geological repository.

Chakravartty described a HEPA filter leaching system (HFLS) used at Idaho Chemical Processing Plant to reduce transuranic and radioactive contaminant levels in the spent HEPA filters [1]. Nitric acid solution of 1 – 3 M strength was used as leachate. The average radiation level (β/ γ) in the post leach filter media for all filters was below 100 mR/ h. Thus the filter leach concept met radiological criteria for disposal as low-level waste. A Filter Leaching System (FLS) has also been developed and operated at Idaho National Engineering and Environmental Laboratory (INEEL) to treat very radioactive, mixed waste HEPA filters [2]. In order to improve the efficiency of FLS, a Pulp Process (PP) has been proposed later [3]. In this process, the filter media and the trapped particles are separated from the filter housing and treated as a pulp. The dissolution of PuO_2 in nitric acid has been difficult to accomplish. The most widespread method of PuO_2 dissolution is based on treatment with a mixture of HNO_3 and HF. The presence of F^- ion raises problems of safe management due to the highly corrosive nature of F^-. The consumption of acid in leaching step will reduce if the particles can be dislodged from the HEPA filter by any mechanical means (ultrasonic vibration, agitation by air etc.).

In the present work a treatment method is developed to decontaminate the HEPA filter to such an extent that further volume reduction by compaction is possible and it can be directly disposed to RCC trenches (RCCT) with less spread of contamination. This method will be more effective when the HEPA filter is loaded with PuO_2. A decontamination factor (DF) of 100 is required for alpha contaminated (glove box generated) HEPA filter so that those will become non alpha in category and further volume reduction in compaction is possible and direct disposal to RCCT, NSDF is permitted. For high surface dose rate (50 R/ h) HEPA filter generated from off gas treatment system requires at least a DF of 250 so that those will available for volume reduction by compaction method.

Experimental

Basic objective of experimental investigation is to reduce the contamination level As Low As Reasonably Achievable (ALARA) so that further volume reduction of the decontaminated filter and direct disposal to NSDF may be possible. Experimental method can be divided into four steps - a) Solid loading in HEPA filter b) Decontamination of HEPA filter by leaching c) Drying of HEPA filter after leaching d) Analysis of dried and decontaminated HEPA filter.

(a) Solid Loading in HEPA Filter

A schematic diagram of HEPA filter loading setup is shown in Figure 1. A rectangular box with flanges was made of stainless steel plate. The open face of the HEPA filter case was placed between flanges of the box. Both sides of the open face of the HEPA filter have closed-cell sponge gaskets composed of synthetic rubber (neoprene). These gaskets were pressed against the flat faces of the flanges by bolted joint to form a leak tight joint. 50 NB Schedule 40 pipes were attached to both sides of the box. The end of one pipe was connected to the inlet of Roots Delfin vacuum pump. A bypass line was made by tee joint and a globe valve was installed in this line to regulate the volumetric air flow rate through the HEPA filter. A provision has been made in the other 50 NB pipe to introduce the solid into the inlet of HEPA filter. A photograph of the solid loading setup is presented in Figure 2. The pressure drop across the HEPA filter (ΔP_{HEPA}) was measured using differential pressure transmitter. The pressure drop data were stored in a paperless recorder, Yokogawa DX 1004-3-4-2. The HEPA filters used in the present work have an initial pressure drop of 21 mmWC at a flow rate of 30 CFM (ft^3/ s) as per the test certificate supplied by manufacturer (M/s. Industrial Filter Corporation). The air velocity in a 50 NB schedule 40 pipe is 6.55 m/ s corresponding to volumetric flow rate of 30 CFM. After switching on the vacuum pump, the air flow rate through filter was kept at desired value by regulating the globe valve. The air velocity was measured using anemometer at 5 points of cross section of the 50 NB pipe as shown in the Figure 3. The average value of these measured velocities is considered. During solid loading the velocity was kept constant by adjusting the opening of the globe valve. The MgO powder (simulant of uranium oxide) was introduced into the 50 NB pipe to produce an aerosol at the inlet of filter. The particle size distribution of MgO was measured using Malvern Mastersizer 3000 laser particle size analyser and shown in Figure 4.

Initial weight of the HEPA filter was noted before placing it inside solid loading setup. Generally a HEPA filter is replaced when the ΔP_{HEPA} is greater than the three times of the initial pressure drop. Hence, solid loading continued until the ΔP_{HEPA} is increased to three times of the initial pressure drop. Figure 5 is showing a typical plot of time versus ΔP_{HEPA}. After completion of solid loading operation the flange joint was opened and final weight of the HEPA filter was taken. The amount of solid loaded into filter was obtained by subtracting initial weight from the final weight.

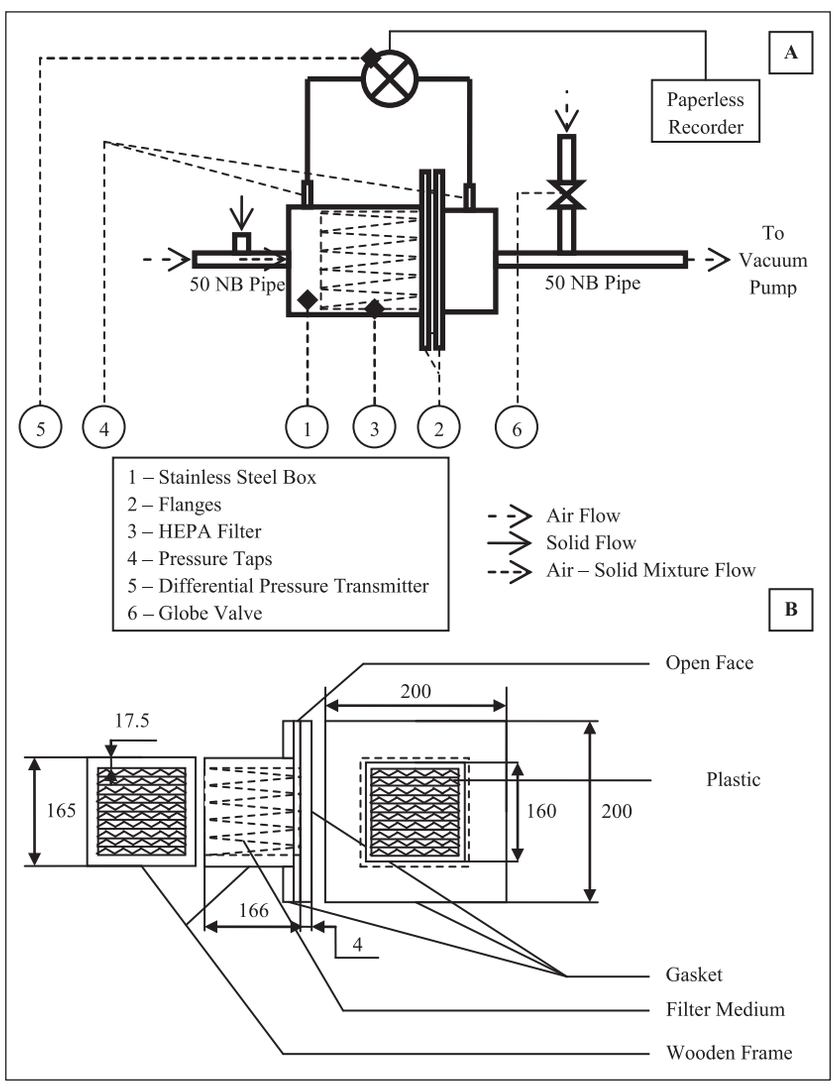

Fig. 1: Schematic diagram of (A) Solid loading setup, (B) HEPA filter

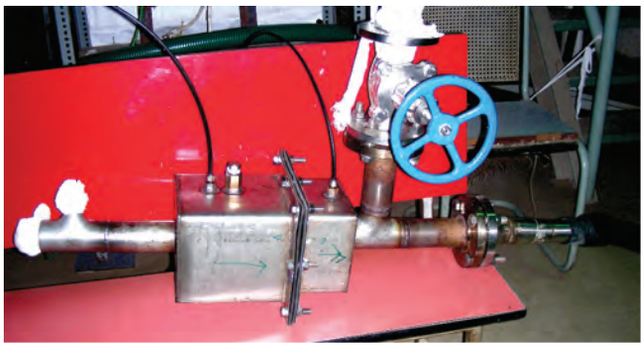

Fig. 2: Photograph of HEPA filter solid loading setup

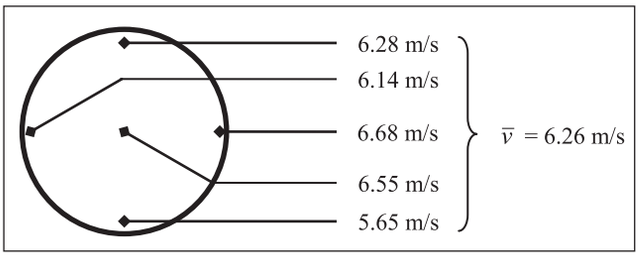

Fig. 3: Five point velocity measurement at the cross section of 50 NB Schedule 40 pipe

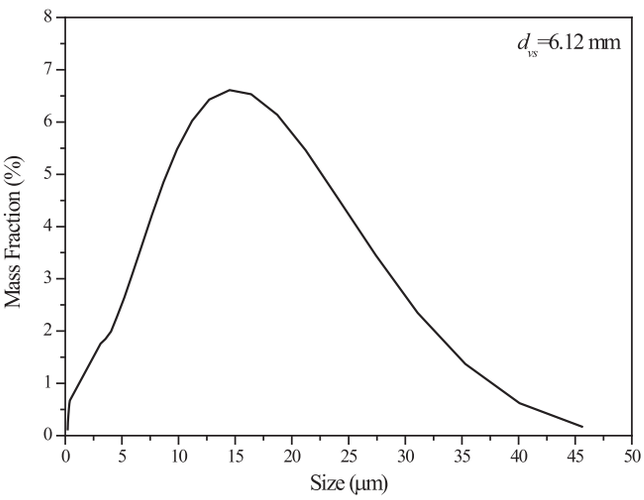

Fig. 4: Particle size distribution of MgO

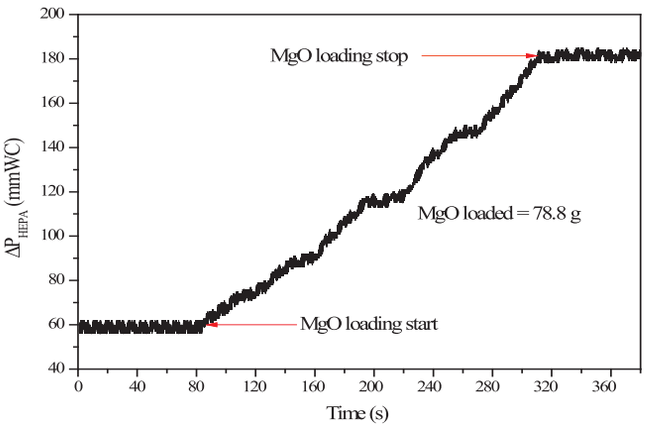

Fig. 5: Time variation of HEPA filter pressure drop during solid loading

(b) Decontamination of HEPA Filter by Leaching

A schematic sketch of the entire leaching system is presented in Figure 6. The leach vessel was fabricated from 304L stainless steel. The solid loaded filter was placed face down in a stainless steel basket. The top lid and bottom surface of the basket were made of 1 mm stainless steel square wire mesh (Figure 7). As the frame of the HEPA filter was made of wood, it can float in leachate. Also the basket holds disintegrated loose filter media during leaching operation and precludes the plugging of the leach vessel drain line.

The basket was kept on the support rod of the leach vessel. Then the cover of the leach vessel was closed by bolted joint. Water was filled into the vessel and the volume of water should just submerge the basket during leaching and rinsing cycles. Leaching of filters includes one leach cycle and one rinse cycle with air sparging. It was found that total 35 l water is required in each cycle. Air sparging was started immediately after filling the leach vessel with water to promote agitation.

(c) Drying of HEPA Filter

The drying operation is performed by forcing hot air through the sparger into the leach vessel. The compressed air supply system consists of a screw compressor and a pressure swing adsorption type air drying unit. The volumetric flow rate (SLPM) of dry air was metered by a rotameter. Then the air was passed through a series of four pre-heaters to obtain desired air temperature. The air temperature at the outlet of the pre-heater was maintained by a PID controller. The temperatures of inlet air and vessel were measured by K type thermocouples. A high temperature humidity meter was procured from M/s. Suntronics Automation and installed in the exhaust line. The measured percentage relative humidity (%RH) data were stored in a paperless recorder. The inbuilt RTD based temperature sensor in humidity transmitter was used to record the exit gas temperature.

The initial moisture content of the dry air was noted before starting the drying operation. After complete drying of HEPA filter, the moisture content of the exit air from leaching vessel will be equal to the initial value and constant. The actual drying time was found out from this indication. Also at the end of each drying experiment, the filter was visually inspected for traces of water. It was confirmed that the moisture content of the exhaust air is a precise indication of complete drying. Time variation in moisture content of the exit air for a particular condition (Dry air flow rate = 36 m^3/ h and Pre-heater set point = 130^{0}C) is presented in Figure 8. The method of determination of drying time from %RH versus time graph is shown in inset of Figure 8. It can be noted that the %RH reached at constant value after completion of drying.

(d) Analysis of Dried and Decontaminated HEPA Filter

After cooling down the basket and HEPA filter to room temperature, the basket was taken out from the leach vessel. The filter was removed from the basket. The basket was thoroughly observed for loose filter medium. The weight of the decontaminated HEPA filter was taken and compared with the initial weight prior to solid loading.

Result and Discussion

The summary of first leaching trial is given in Table 1. The first trial results indicated that the method of leaching should be

modified. The liquid does not permeate easily through the filter. The filter media retains considerable amount leachate/ rinsate (Figure 9). After drying operation, the solids remained in this leachate/ rinsate again deposited in the filter. Also a very long time is required for drying of the filter media. Hence, the filter media should be breached prior to leaching, to aid in the leaching process. Breaching of filter media also reduces the drying time significantly. Air sparging might be necessary to promote agitation. It was also noted that at a higher sparging rate, i.e., 288 SLPM complete removal of loaded solid is possible without adding any acid. At the end each cycle, the basket and drained liquid was thoroughly checked for any loose filter media. No, loose filter media was observed in both the basket or drained liquid.

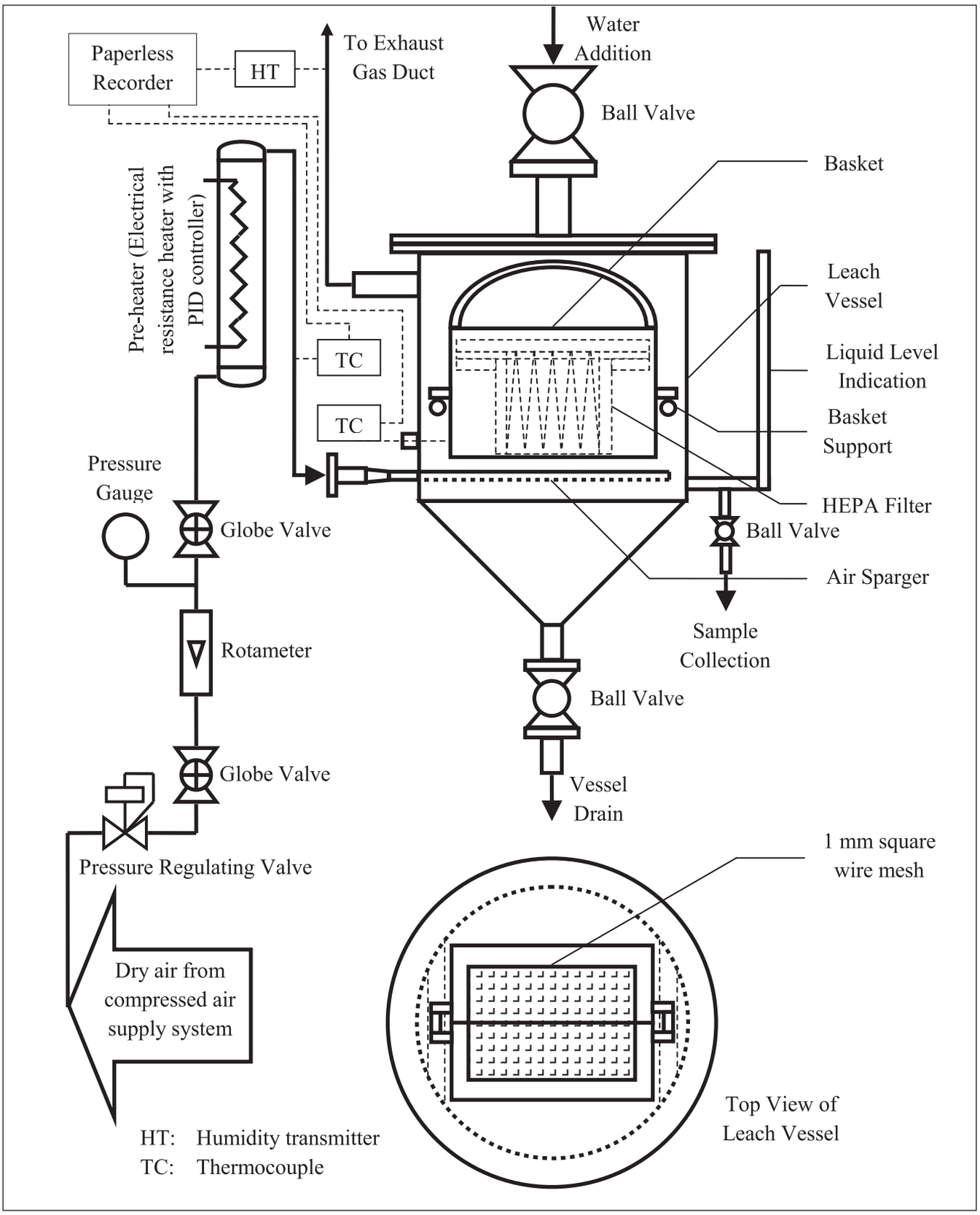

Fig. 6: Schematic diagram of HEPA filter leaching and drying system

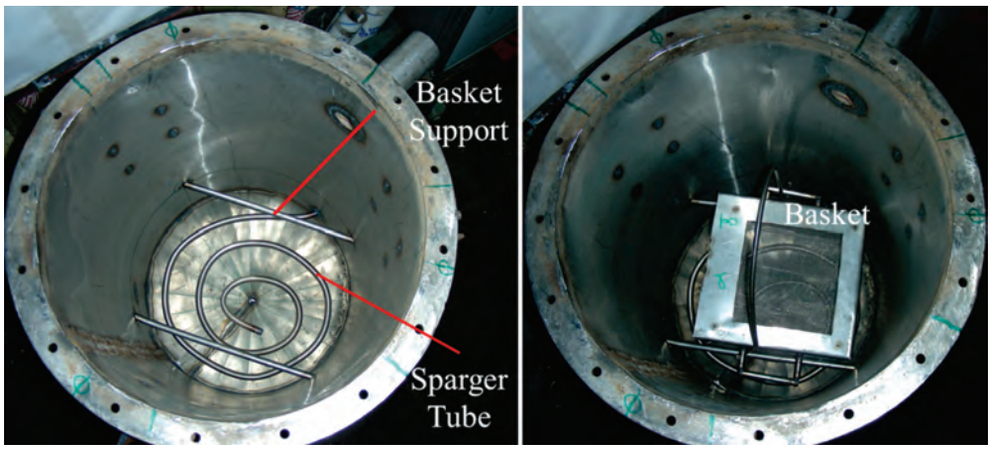

Fig. 7: Photograph of inside of leach vessel and basket

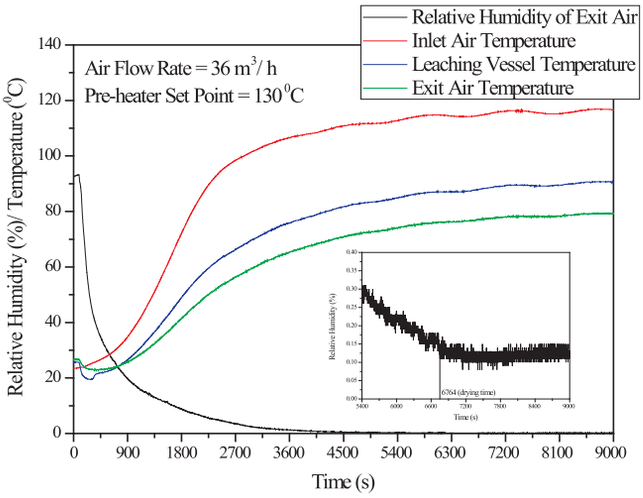

Fig. 8: Plot of inlet air, leach vessel and exit air temperature and exit air %RH as a function of time for a particular condition

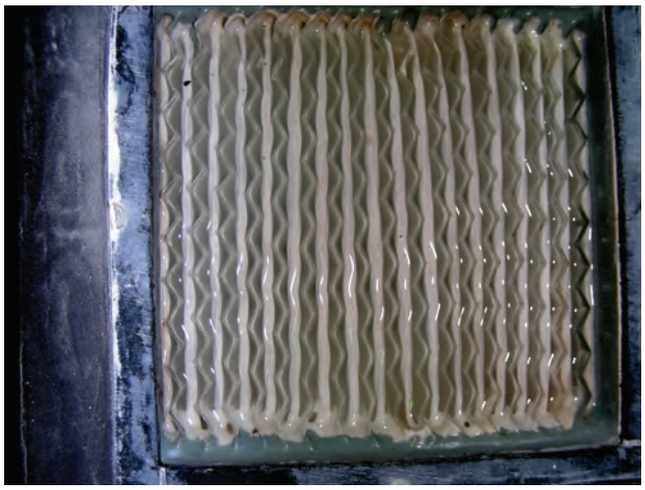

Fig. 9: Retention of leachate by HEPA filter

Table 1: Summary of first leaching trial

Experiment No. 1		
Air flow rate during solid loading		18.3 CFM
Amount of MgO loaded into HEPA filter		132.2 g
Duration of	leaching cycle – 1	1 hr.
	rinsing cycle – 1	1 hr.
Air sparging rate for 1st cycle		144 SLPM (5 SCFM)
Observation after draining the rinsate		Corrugated structure of HEPA filter holds considerable amount solution
Drying time		12 hr. (at air flow rate of 1000 SLPM at 140^{0}C)
MgO remained in filter		64.2 g
Modification in method		Filter is mechanically breached
Duration of	leaching cycle – 2	1 hr.
	rinsing cycle – 2	1 hr.
Air sparging rate for 2nd cycle		144 SLPM (5 SCFM)
Drying time		< 1 hr. (at air flow rate of 1000 SLPM at 140^{0}C)
MgO remained in filter		41.2 g
Duration of	leaching cycle – 3	1 hr.
	rinsing cycle – 3	1 hr.
Air sparging rate for 3rd cycle		288 SLPM (10 SCFM)
Drying time		< 1 hr. (at air flow rate of 1000 SLPM at 140^{0}C)
MgO remained in filter		Nil

In the next experiments the breaching operation and higher purging rate were applied and duration of leaching and rinsing cycle was optimized. The results of next two experiments are presented in Table 2. It can be concluded from Table 2 that one 60 minutes leach cycle followed by one 60 minute rinse cycle with a sparging rate of 10 SCFM (288 SLPM) required for complete dislodging the solid from HEPA filter.

Total 24 number experiments were carried out to generate the drying time data for different air flow rates (30 – 60 Nm^3/ h) and air temperatures (110 – 140^{0}C). A complete set of drying time data for a HEPA filter having 0.53 m^2 surface area was generated and presented in Figure 11. It was observed that the time required for complete drying of filter decreases with increase in volumetric air flow rate and temperature. This is on account of the enhanced heat and mass transfer.

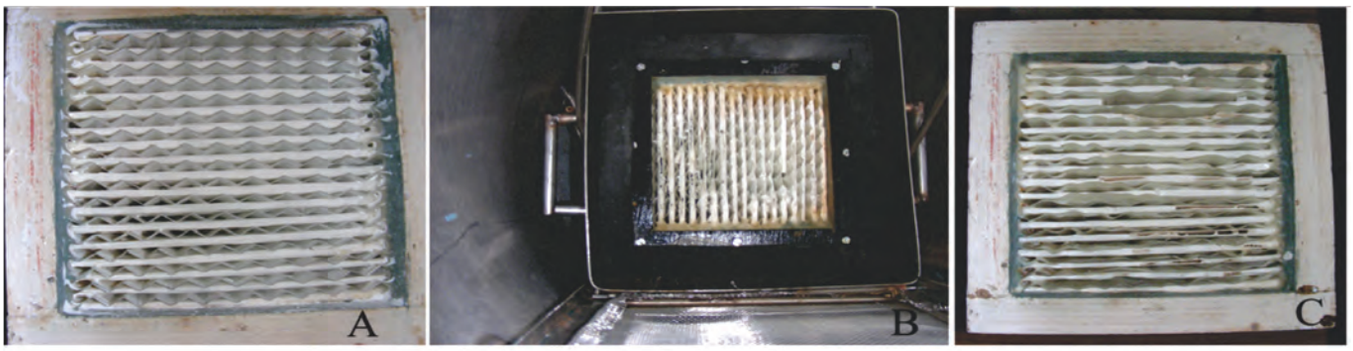

Fig. 10: Photograph of HEPA filter (A) after MgO loading, (B) after breaching (C) after leaching and drying

Table 2: Optimization of duration of leaching and rinsing cycle

Experiment No. 2		
Air flow rate during solid loading		28.7 CFM
Amount of MgO loaded into HEPA filter		78.8 g
Duration of	leaching cycle – 1	1 hr.
	rinsing cycle – 1	1 hr.
Air sparging rate		288 SLPM (10 SCFM)
Drying time		< 1 hr. (at air flow rate of 1000 SLPM at 140^{0}C)
MgO remained in filter		Nil
Experiment No. 3		
Air flow rate during solid loading		28.7 CFM
Amount of MgO loaded into HEPA filter		77 g
Duration of	leaching cycle – 1	45 min.
	rinsing cycle – 1	45 min.
Air sparging rate		288 SLPM (10 SCFM)
Drying time		< 1 hr. (at air flow rate of 1000 SLPM at 140^{0}C)
MgO remained in filter		8.2 g

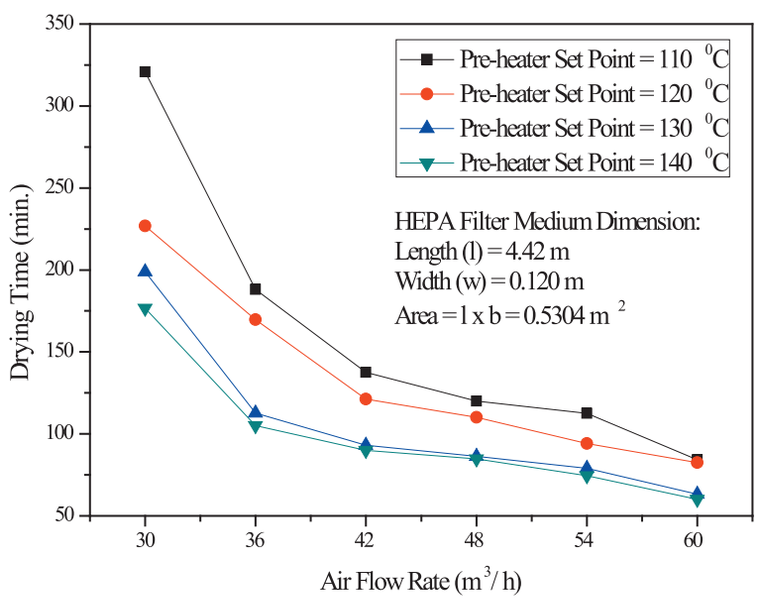

Fig. 11: Influence of air flow rate and inlet air temperature on drying time

Estimation of Decontamination Factor

Initially the quantity of MgO remained in the treated HEPA filter was estimated by simply measuring the weight of HEPA filter. In the later stage, more precise estimation has been carried out by chemical analysis of leachate and rinsate. After collecting the leachate and rinsate from the leach vessel, nitric acid was added for complete dissolution of suspended MgO particles. The liquid samples of leachate and rinsate were analysed in an Inductively Coupled Plasma Optical Emission Spectroscopy (Make: Horiba Scientific). The quantity of Mg present in leachate and rinsate is given in Table 3. The total quantity of Mg removed from HEPA filter was obtained and it was converted to equivalent weight of MgO. The quantity of MgO remained in the HEPA filter was determined by subtracting the equivalent weight of MgO in leachate and rinsate from amount of MgO initially loaded into HEPA filter. A DF is estimated from the ratio of quantity of MgO prior to after treatment of HEPA filter.

Table 3. Estimation of Decontamination Factor

Experiment No4		
Air flow rate during solidoading		28.7 CFM
Amount of MgO loaded into HEPA filter		75.1 g
Duration of	leaching cycle– 1	1 hr.
	rinsing cycle– 1	1 hr.
Air sparging rate		288 SLPM (10 SCFM)
Volume of leachate		35 l
Volume of rinsate		35 l
Mg content of leachate		1.053 g/ l
Mg content of rinsate		0.2195 g/ l
Total Mg removed from HEPA filter		(1.053 + 0.2195) × 35 = 44.5375 g (≈ 74.23 g MgO)
MgO remained in HEPA filter		75.1– 74.23= 0.87 g
Decontamination Factor		75.1/0.87= 86.32

Conclusion

A methodology has been developed for decontamination of HEPA filter. After completion of several trials on leaching and drying of HEPA filters, the following conclusions were drawn:

- The filter media should be breached for effective leaching and rinsing operations. In future, a remotely operated mechanical tool shall be developed for this breaching operation.
- The filter should be placed in a basket to prevent plugging of the drain line due to loose filter media. However, loose filter media was not observed in any trials.
- It was found that one 60 minutes leach cycle followed by one 60 minutes rinse cycle with a sparging rate of 10 SCFM (288 SLPM) required for complete dislodging the solid from HEPA (200 mm × 170 mm × 150 mm) filter. Nevertheless, it is applicable for small size HEPA filter mostly used in glove box. The methodology can be exercised to find out optimum duration and number of cycles required to decontaminate other sizes of filters.
- During HEPA filter leaching operation, acid was not used. It may improve the leaching operation by lowering the sparging air rate as well as leaching time. The future experiments can be planned considering acid leaching. Another objective of not to use acid was to check the mechanical washing efficiency by the means of air sparging which may be helpful for alpha (Pu) decontamination.
- The quantity of MgO removed from HEPA filter was estimated precisely from chemical analysis of leachate and rinsate. A DF is defined as the ratio of quantity of MgO prior to after treatment of HEPA filter and the value of DF was found to be 86.32.
- It was observed that the time required for complete drying of filter decreases with increase in volumetric air flow rate and temperature. The hot air flow rate shall be kept as low as possible to prevent the carryover/ entrainment of any active particles. The low air flow rate will also minimize the off-gas load. A lower temperature shall be selected for drying air to minimize the power consumption in the drying operation and minimizing the heat load in the off gas treatment process. The choice of air flow rate and temperature depends on the processing time available per filter.
- In future, additional experiments will be planned to decrease the volume of leachate and rinsate by reusing them in next leaching and rinsing cycles.

Acknowledgement

Authors are extremely grateful to Shri K. V. Ravi, CE, NRB and Dr. (Smt.) Sadhana Mohan, Associate Director, ChEG for their valuable support and motivation for the entire work. The authors are thankful to all FRWMD design team especially Shri U. K. Mukherjee, Ms. Anjali & Shri Ramakant (TDD, NRG) for their instrumentation, design, fabrication and feed preparation support and all staff of CEL - III, ChED for fabrication, instrumentation and conduction of experiments. Authors are also thankful to Dr. S.K. Musharaf Ali, Head, LSS, ChED and Shri A.K. Singha Deb for chemical analysis of leachate and rinsate.

References

1. Ambika C. Chakravartty, "HEPA Filter Leaching Concept Validation Trials at the Idaho Chemical Processing Plant", INEL-95/0182, April 1995.
2. M. Argyle, R. Demmer, K. Archibald, K. Brewer, K. Pierson, K. Shakelford, K. Kline, "INEEL HEPA Filter Leach System: A Mixed Waste Solution", INEEL, WM'99 Conference, February 28 – March 4, 1999,Tucson, AZ.
3. J. S. Hu, "Development of a Pulp Process for Treating Contaminated HEPA Filters(II)", INEEL, WM'01 Conference, February 25 – March 1, 2001, Tucson, AZ.

Modelling of Mass Transfer in AnnularPulsed Disc and Doughnut Column

Sourav Sarkar, K.K. Singh and K.T. Shenoy
Chemical Engineering Division

Air pulsed columnsare commonly used forcarrying out solvent extraction in the back-end of the nuclear fuel cycle. This work is aimed at modelling of mass transfer inone of the designs of air pulsed column i.e.Annular Pulsed Disc and Doughnut Column (APDDC) which comprises of disc and doughnut shaped plates stacked in an annulus.The model, which is based on axial dispersion model (ADM), has been validated with the data of uranium extraction reported in literature. Auser-friendly graphical user interface (GUI) for the model is developed. The model with GUI serves as a simulator. The inputs required in the simulator are the operating conditions and geometrical parameters of APDDC. The outputs of the simulator are theexit concentrations of the solute(s) in the aqueous phase and organic phase and concentration profiles of the solute(s) in both phases inside the column. The simulator has been used to understand the effects of operating and geometrical parameters on mass transfer in APDDC.

Keywords: axial dispersion, disc and doughnut, mass transfer, pulsed column, solvent extraction

Introduction

PUREX process is widely used for reprocessing of spent nuclear fuel. For this, air pulsed columns are preferred over other contactors like mixer-settler, rotating disc column, centrifugal extractor etc. as they do not have mechanical moving parts that may require maintenance but still provide high throughput and high separation efficiency[1,2,3,4]. Though pulsed sieve plate columns (PSPCs) have been traditionally used for spent nuclear fuel reprocessing, pulsed disc and doughnut columns (PDDCs) have been proposed as an alternative to pulsed sieve plate columns [5,6,7]. Advantages such as better solid handling capability and higher dispersed phase holdup resulting in better mass transfer make PDDCs attractive[8,9].A further modification in design is use of annulus instead of a cylindrical column so that high surface to volume ratio can be ensured to take care of criticality hazard. Such a column is called as annular pulsed disc and doughnut column (APDDC). There ported studies on liquid-liquid two-phase flow and mass transfer in APDDCs are very few. Liu et al, 2015 and Liu et al., 2015a have reported experimental results on dispersed phase holdup, Sauter mean drop diameter, axial dispersion and mass transfer in APDDC[7,10].Nabeshima, 1991 reported concentration profile of uranium in the aqueous phase for uranium extraction from 3N nitric acid solution inan APDDC[11].

In the present work, a code to estimate mass transfer in APDDC has been written and validated with the experimental data of Nabeshima, 1991 [11]. The code is based on axial dispersion model. A graphical user interface (GUI) of the code is also developed. The validated code with GUI serves as a simulator. This simulator has been used for parametric analysis to gain insights into how the operating and geometric parameters affect the mass transfer in APDDC. Though axial dispersion model based mass transfer codes such as PULCO and DYNAC have been reported for other designs of pulsed columns, to the best of our knowledge, axial dispersion model based mass transfer code for APDDC has not been reported so far.

Modelling

The model equations describing the variation of concentration of i^{th} solute over a differential height in the aqueous and organic phases are given by Eq. (1) and Eq. (2), respectively.

$$E_x \frac{d^2 c_{ix}}{dz^2} - V_x \frac{dc_{ix}}{dz} - k_{ioy}\, a\left(c_{iy} - c_{iy}^*\right) = 0 \quad (1)$$

$$E_y \frac{d^2 c_{iy}}{dz^2} + V_y \frac{dc_{iy}}{dz} + k_{ioy}\, a\left(c_{iy} - c_{iy}^*\right) = 0 \quad (2)$$

E_x and E_y are the axial dispersion coefficients for the aqueous phase and the organic phase, respectively. The aqueous phase is considered as the dispersed phase while organic phase is considered as the continuous phase, as is usually the case for the column in which fission products are separated from major actinides[11,7,10]. V_x and V_y are the superficial velocities of the aqueous and organic phases, respectively. k_{ioy} is the overall mass-transfer coefficient for i^{th} solute. a represents the specific interfacial area for mass transfer. c_{ix} and c_{iy} are the concentrations of i^{th} solute in the aqueous phase and organic phase, respectively. z is the height measured from the bottom of the column. To solve Eqs. 1 & 2, correlations to estimate axial dispersion coefficients, dispersed phase holdup, Sauter mean drop diameter, mass transfer coefficient and equilibrium data are required. For this, correlations and equilibrium data reported in literature, referred to in Table 1,are used. The correlations are for 30% TBP in dodecane and 3N nitric acid system. Equilibrium data is for major actinides and takes into account the acid concentration. The correlations used in the model have been tested for columns having up to 0.254 m outer diameter by Liu, et al., 2016 [14] . For larger diameter columns, scale-up criteria proposed by Liu, et al., 2016 [14] is followed. The model equation are discretised with finite element formulation using quadratic shape function. For solving resulting linear discretised set of equations, Gauss-Seidelmethod is used.

Table 1: Correlations used in the model

Correlation	Source
Axial dispersion coefficient	Charton, et al., 2012[12]
Dispersed phase holdup	Liu, et al., 2015 [7]
Sauter mean drop diameter	Liu, et al., 2015 [7]
Mass transfer coefficient	Liu, et al., 2015a [10]
Equilibrium relation	Geldard et al., 1985 [13]

Validation

The model is validated with the experimental data reported by Nabeshima, 1991 [11] for organic continuous mode of operation of APDDC. The column has 0.12m inner diameter and 0.2 m outer diameter. Column height is 6m. Inlet concentration of uranium in the aqueous phase is 260 gm/lit, and aqueous and organic phase flow rates are 564lph and 275lph, respectively. Fractional open area and disc to doughnut spacing are 25%and 0.02m, respectively. Fig.1 shows the comparison of experimental and predicted uranium concentration profile in the aqueous phase along the column height. A good agreement between simulation results and experimental values can be observed. The average absolute relative error is about 10%.

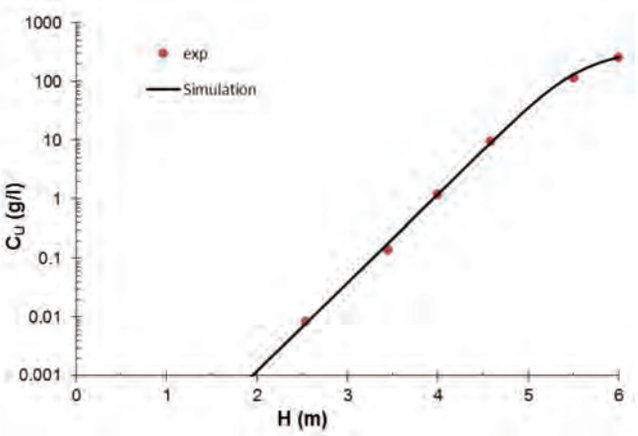

Fig. 1: Comparison of predicted and experimental concentration profile of uranium in aqueous phase in APDDC. Experimental data are from Nabeshima,1991[11]

Simulator with GUI

After validating the model, the graphical user interface (GUI) of the code was developed. The code with GUI serves as a simulator and has been named as ColSim: APDDC. The simulator, which embeds the correlations and equilibrium data reported in literature, can be used for estimating mass transfer of major actinides in APDDC operated in organic continuous mode. The inputs required are aqueous phase input parameters (concentration of solute(s) in the incoming aqueous phase, flow rate), organic phase input parameters (concentration of solute(s) in the incoming organic phase, flow rate), pulsing parameters (pulsing amplitude and frequency), physical properties (continuous and dispersed phase density, viscosity, interfacial tension) and geometric parameters (inner, outer diameters of the column, fractional open area, disc to doughnut distance and column height). The outputs of the simulator are the concentration of the solute(s) in the leaving aqueous and organic phases and concentration profile of the solute(s) in the aqueous and organic phases inside the column. The simulator can be used to understand the dependence of the operating and geometric parameters on the mass transfer performance of APDDC. A snapshot of the GUI of the simulator is shown in Fig. 2. Table 2 lists the typical inputs provided in the windows that open when the boxes in the GUI are clicked.

Parametric Analysis

Effects of operating parameters

The simulator embedding the validated model was used for parametric analysis to understand the effects of operating parameters i.e. dispersed phase flow rate, continuous phase flow rate and pulsing velocity on mass transfer in APDDC. It is assumed that the correlations listed in Table 1 hold good in the range of the operating parameters covered in this parametric analysis. Fig. 3(a) shows the effect of dispersed phase flow rate on concentration profile of uraniumin the aqueous phase for the case of uranium extraction from aqueous phase to organic phase in APDDC when other operating conditions and

Table 2: Typical inputs provided to the simulator

Aqueous Input Parameters		**Organic Input Parameters**	
Aqueous phase velocity (m/s)	0.0038	Organic phase velocity (m/s)	0.0078
Concentration of component 1 (gm/lit)	10	Concentration of component 1 (gm/lit)	0
Concentration of component 2 (gm/lit)	260	Concentration of component 2 (gm/lit)	0
Acid concentration (N)	3	**Geometrical Parameter**	
Physical Properties		Outer diameter of column (m)	0.2
Dispersed phase density (kg/m^3)	1090.8	Inner diameter of column (m)	0.12
Continuous phase density (kg/m^3)	931.5	Fractional open area (-)	0.25
Dispersed phase viscosity (Pa.s)	0.0018	Distance between disc and doughnut (m)	0.02
Continuous phase viscosity (Pa.s)	0.00098	Column height (m)	6
Interfacial tension (N/m)	0.014	**Pulsing Parameters**	
Temperature (K)	300	Amplitude of pulsing (m)	0.02
		Frequency of pulsing (Hz)	0.83

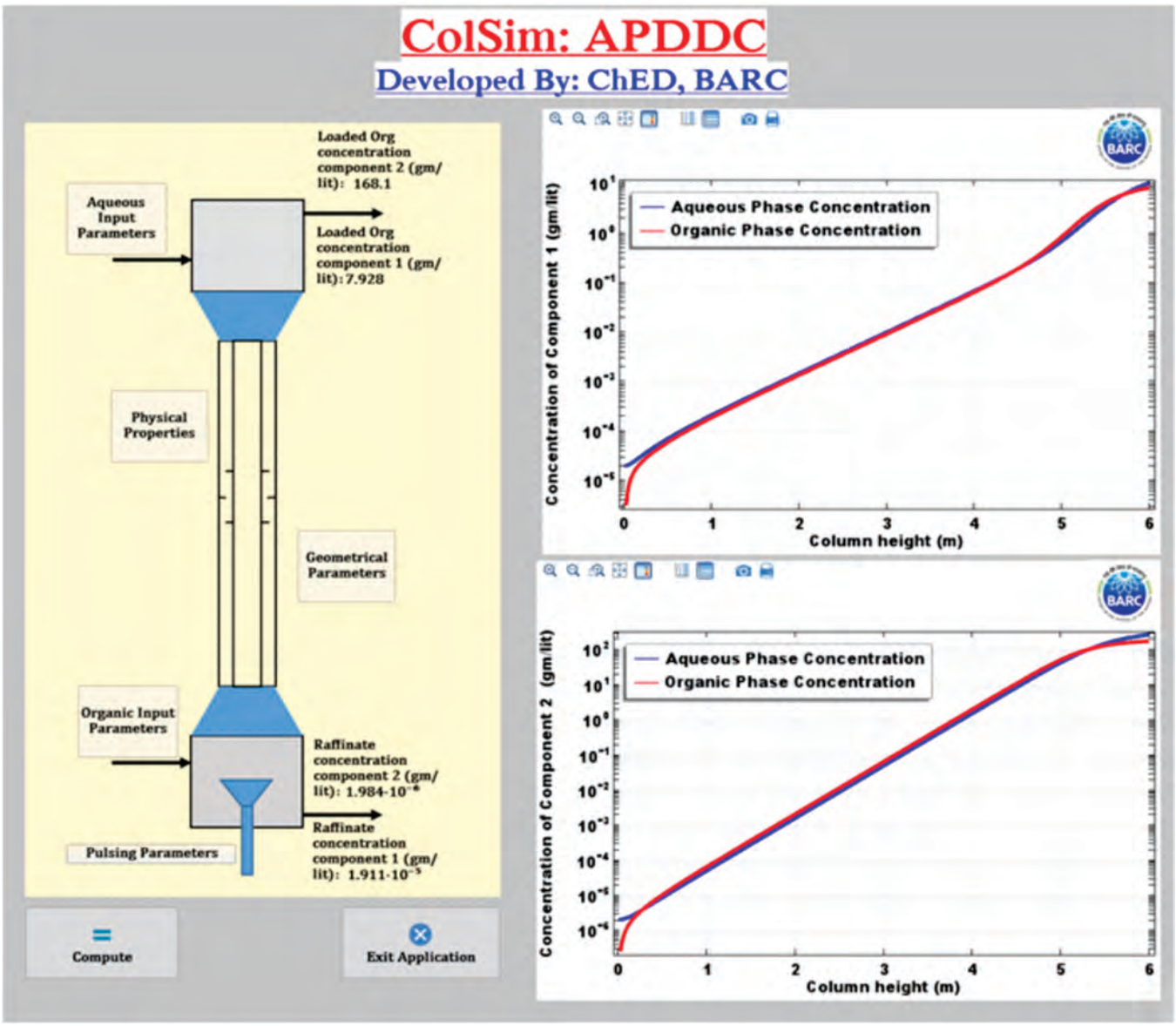

Fig.2 : Graphical user interface of the simulator ColSim: APDDC

geometric parameters are kept unchanged. Fig. 3(a) shows that mass transfer is enhanced when flow rate of dispersed phase is increased. An increase in dispersed phase flow rate causes increase in dispersed phase holdup and specific interfacial area which reflects in better mass transfer. However, with continued increase in dispersed phase flow rate with a constant flow rate of the continuous phase, the capacity of the continuous phase to pick up the solute from the dispersed phase tends to saturate. This results in only marginal increase in mass transfer with continued increase in dispersed phase flow rate.

Fig. 3(b) shows the effect of continuous phase flow rate on concentration profile of uranium in the aqueous phase inside APDDC when other operating conditions and geometric parameters are kept constant. As observed for the case of the effect of dispersed phase flow rate, mass transfer is found to increase with an increase in continuous phase flow rate. An increase in continuous phase flow rate is known to increase dispersed phase holdup in pulsed columns. This is because a higher flow rate of continuous phase increases the drag force acting on the dispersed phase droplets. This causes enhanced retention of the dispersed phase drops in the column causing dispersed phase holdup and hence specific interfacial area to increase. Thus mass transfer is improved when continuous phase flow rate is increased.

Fig. 3(c) shows the effect of pulsing velocity (pulsing velocity is changed by changing pulsing frequency) on concentration profile of uranium in APDDC when other operating conditions and geometric parameters are kept constant. Pulsing velocity is observed to have a significant influence on mass transfer with mass transfer increasing with increase in pulsing velocity. Increase in pulsing velocity is known to cause dispersed phase holdup to increase and Sauter mean drop diameter to decrease in air pulsed columns. Both these factors lead to enhancement of mass transfer with increase in pulsing velocity.

Effect of column outer diameter

After studying the effects of operating parameters on mass transfer in APDDC, ColSim: APDDC was used to understand the effect of column outer diameter on mass transfer. For

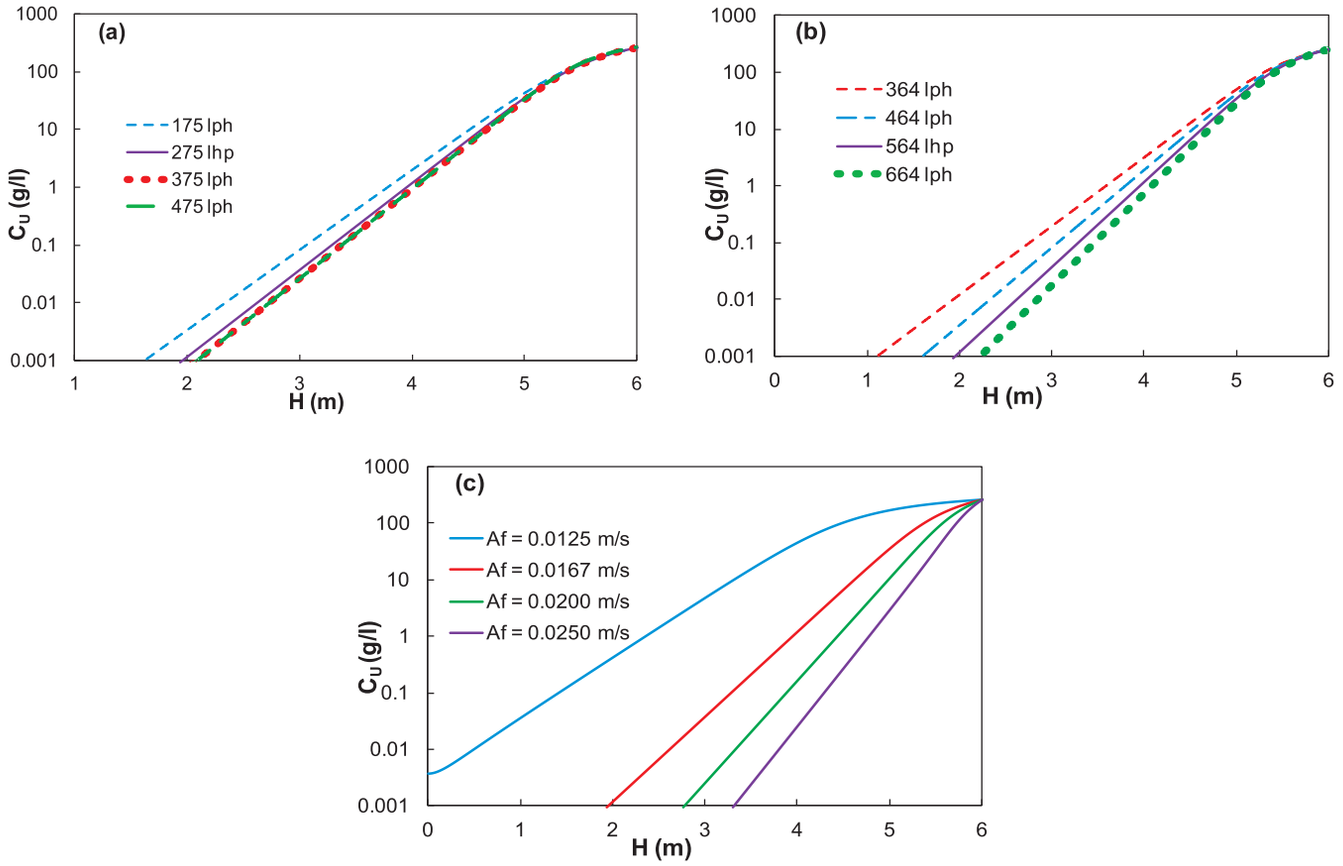

Fig. 3: Effect of (a) dispersed phase flow rate,(b) continuous phase flowrate and (c) pulsing velocity on concentration profile of uranium in the aqueous phase inside APDDC for extraction of uranium from aqueous phase (dispersed) to organic phase.

increasing the column diameter, the scale-up scheme proposed by Liu, et al., 2016[14]is followed. In this scheme, the ratio of disc and doughnut spacing and column annular gap is kept constant when the column diameter is increased. Pulsing amplitude is kept equal to disc and doughnut spacing and frequency of pulsing is changed to keep pulsing velocity same. Continuous and dispersed phase velocity are kept constant. Outer diameter of the column is increased from 0.2 m to 0.26m keeping inner diameter constant at 0.12m.Fig. 4a shows the uranium concentration profile in the aqueous phase along the column height for columns of different diameters. It is observed that with increase in column outer diameter, height of the column required to get the same degree of separation increases. A case of major actinide co-extraction was simulated for different outer diameters of the column. To achieve more than 99.9% extraction of the major actinides from aqueous phase to organic phase, column height required for different values of outer column diameters is estimated and shown in Fig. 4b. It is observed that column height required for more than99.9% recovery of major actinides from the aqueous feed solution increases with increase in outer column diameter. This can be attributed to increase in axial dispersion with increase in outer column diameter.

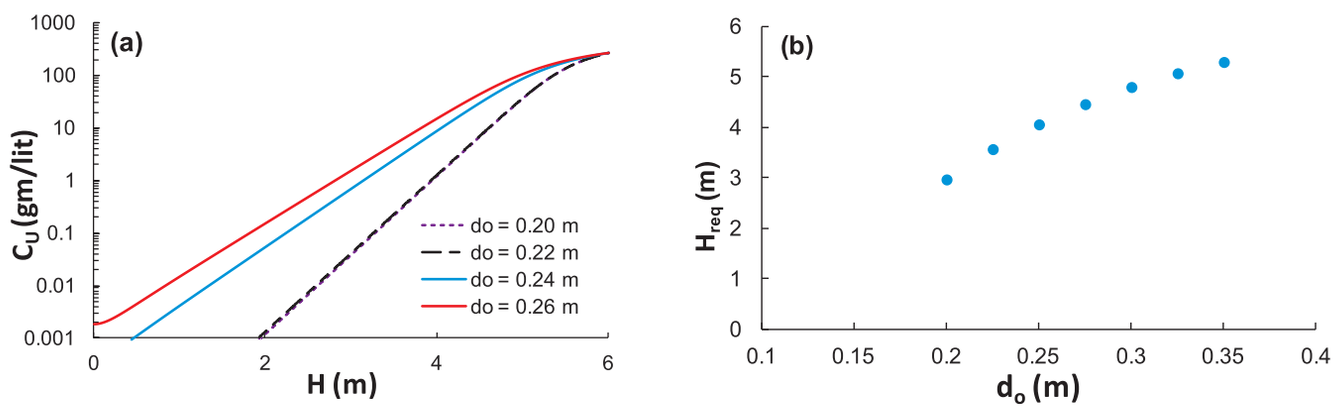

Figure :(a) Effect of column outer diameter on the concentration profile of uranium in the aqueous phase inside APDDC (b) Variation of column height required for more than 99.9% extraction of major actinides for different values of outer column diameter

Conclusion

An axial dispersion based model for estimating mass transfer performance of Annular Pulsed Disc and Doughnut Column(APDDC) has been developed and validated with the experimental data reported in literature on uranium extraction in APDDC. The model embeds the correlations reported in literature for estimating hydrodynamic variables such as Sauter mean diameter, dispersed phase holdup and axial dispersion coefficient. A user-friendly graphical user interface (GUI) of the model has also been developed. The simulator thus developed has been named as CoLSim: APDDC. The simulator has been used for parametric analysis to understand the effects of operating conditions and column outer diameter on the mass transfer performance of APDDC. Within the range of parameters explored, the mass transfer performance of APDDC is found to be better on increasing dispersed phase velocity or continuous phase velocity or pulsing velocity. The effect of pulsing velocity is the most pronounced among the operating parameters. The simulator is also used to estimate the effect of column outer diameter on mass transfer performance. It shows that mass transfer performance deteriorates when column outer diameter is increased. Therefore, the height required to achieve the desired degree of separation increases with increase in outer column diameter.

References

1. Chaturabul, S. et al., 2012. Arsenic removal from natural gas condensate using a pulsed sieve plate column and mass transfer efficiency. Separation Science and technology, 47(3), pp. 432-439.
2. Ferreira, et al., 2010. Extraction of copper from acidic leach solution with Acorga M5640 using a pulsed sieve plate column. Hydrometallurgy, 104(1), pp. 66-75.
3. Gameiro, et al., 2010. Copper extraction from ammoniacal medium in a pulsed sieve-plate column with LIX 84-I. Journal of hazardous materials, 183(1), pp. 165-175.
4. Schön, J., Schmieder, H. & Kanellakopulos., B., 1990. Operating Experience with Minka: U-Pu Separation in the Presence of Technetium with an Organic Continuous Pulsed Column. Separation Science and Technology, 25(13-15), pp. 1737-1750.
5. Torab-Mostaedi, M., Ghaemi, A., Asadollahzadeh, M. & Pejmanzad, P., 2011a. Mass transfer performance in pulsed disc and doughnut extraction columns. Brazilian Journal of Chemical Engineering, 28(3), pp. 447-456.
6. Wang, Y. Y., Shan, J. I. N. G., Wu, G. L. & Wei, W. U., 2006. Axial mixing and mass transfer characteristics of pulsed extraction column with discs and doughnuts.. Transactions of Nonferrous Metals Society of China, 16(1), pp. 178-184.
7. Liu, J. Q., Li, S. W. & Jing, S., 2015. Hydraulic Performance of an Annular Pulsed Disc-and-Doughnut Column. Solvent Extraction and Ion Exchange, 33(4), pp. 385-406.
8. Movsowitz, R. L., Kleinberger, R., Buchalter, E. M. & Grinbaum, B., 2000. Comparison of the performance of full scale pulsed columns vs. mixer-settlers for uranium solvent extraction. Uranium 2000: International symposium on the process metallurgy of uranium.
9. Jahya, A. B., Stevens, G. W. & Pratt, H. R., 2009. Pulsed discs- and-doughnut column performance. Solvent extraction and ion exchange, 27(1), pp. 63-82.
10. Liu, J. Q., Li, S. W. & Jing, S., 2015a. Axial Mixing and Mass Transfer Performance of an Annular Pulsed Disc-and-Doughnut Column. Solvent Extraction and Ion Exchange, 33(6), pp. 1-15.
11. Nabeshima, M., 1991. Analysis of cylindrical and annular pulsed columns with different internal plates in the PUREX process. Nuclear technology, 95(2), pp. 207-218.
12. Charton, S., Duhamet, J., Borda, G. & Ode, D., 2012. Axial dispersion in pulsed disk and doughnut columns: A unified law. Chemical Engineering Science, Volume 75, pp. 468-477.
13. Geldard, J. F., Phillips, L. & Beyerlein, A. L., 1985. Correlation functions for the distribution coefficients of U (IV) and Pu (III) ions between aqueous nitric acid and 30% TBP in an aliphatic diluent. Nuclear technology, 70(3), pp. 394-400.
14. Liu, J. Q., Li, S. W. & Jing, S., 2016. Scale-Up Study on the Performance of Annular Pulsed Disc-and-Doughnut Columns. Solvent Extraction and Ion Exchange, 34(5), pp. 485-501.

Radiation Induced Mutations for Developing Enhanced Resistance to Yellow (stripe) Rust of Wheat

Vishwakarma G. and Das B.K.
Nuclear Agriculture & Biotechnology Division, BARC, Mumbai - 400 085
Kumar S. and Mishra C.N.
ICAR-Indian Institute of Wheat & Barley Research, Karnal, Haryana- 132001
Saharan M.S.
Department of Plant Pathology, ICAR-Indian Agricultural Research Institute, New Delhi- 110012
Saini A.
Molecular Biology Division, BARC, Mumbai - 400 085

Wheat production worldwide and in India is threatened by yellow (stripe) rust disease of wheat. Recently, new aggressive and virulent races of yellow rust overcoming resistance present in widely grown wheat varieties has re-emphasized importance for constant breeding efforts for resistance to rust disease. Here, we report gamma ray induced mutation breeding for development of wheat mutant lines in the variety DBW-88 showing enhanced resistance to virulent races of yellow rust. The yellow rust resistant lines are being tested for yield and other agronomic traits. Overall, mutation breeding can be used for development of disease resistant genetic resources, and also excellent mutant models for understanding molecular mechanism of rust resistance in wheat.

Introduction

Wheat is the second most important cereal produced worldwide. With global production close to 750 million tons, wheat is cultivated yearly on 215 million hectares of land, accounting for 50 billion USD trade globally[1]. It acts as food for ~ 2.5 billion people spread across 89 countries. Wheat is the second most important crop after rice in India with annual production well above 90 million tons consistently and caters as staple diet for half of Indian population, providing vital source of vegetarian protein, microelements and vitamins. With introduction of semi dwarf wheat cultivars and sustained breeding efforts, India attained self-sufficiency in wheat production and now it also exports the surplus production. The ever increasing population of India demands higher food grain production. It is estimated that India needs to double its wheat production by 2050, with constraints of adverse climate, reduced agricultural inputs to feed its ever growing population.

Wheat Rust Diseases

Wheat production in India is challenged by many biotic (by living organism) and abiotic (by non-living organism) stresses, affecting its yield and seed quality. Wheat rust diseases are one of the most devastating and deleterious diseases of wheat, caused by fungal pathogen of Puccinia genus and are of three types viz., stem rust or black rust (caused by *Puccinia graminis* f.sp. *tritici*), leaf rust or brown rust (caused by *Puccinia triticina*) and stripe rust or yellow rust (caused by *Puccinia striiformis*)[2] (Fig. 1). Wheat yellow (stripe) rust is one of the most deleterious diseases having potential to cause 100% loss in yield. Although, it is mostly considered a disease of cooler and hilly areas it has become a major concern in the north western plains zone of India (NWPZ) (Punjab, Haryana, Delhi and Western Uttar Pradesh) which contribute 70% of Indian wheat production. Globally, it is predicted that 88% of world wheat production is susceptible to stripe rust and would be the most important biotic concern for global wheat production.

Fig. 1: Phenotypic symptom of infection of (A): wheat stem/black rust, (B): wheat leaf/brown rust, (C): wheat stripe/yellow rust.

Emergence of new virulent yellow (stripe) rust races & Breeding strategies

Historically, there have been many incidences of yellow rust epidemics, leading to change in coverage of varieties in the countries. For example, in 1970s resistance by *Yr2* was overcome in North Africa, Indian Subcontinent, Middle East, East African highlands and China, which was present in almost all the prevalent varieties[4]. Similarly in 1990, *Yr9* was broken down which led to epidemics in Asia[5]. New races *PstS1* and *PstS2* had emerged in Middle East and Central Asia and had adapted better to high temperature with novel virulence spectrum wiping out the native races[6]. Most recently, the Pst "Warrior" race which appeared in 2011 on the wheat variety 'Warrior' in Europe required complete replacement of the variety[7].

In India yellow rust epidemics have been reported since 1982 in Punjab, Haryana, Western Uttar Pradesh and Jammu & Kashmir[8]. Apart from breakdown of *Yr2* in Indian varieties, virulent races of Pst viz 46S119 and 78S84 emerged in 1995 overcoming resistance to *Yr9* and *Yr9* + *Yr27* [9]. Race 78S84 compelled government and farmers to replace most popular variety PBW-343 from almost 70% of wheat cultivated area in India. Most recently a new Pst pathotype 110S119 emerged overcoming resistance in widely cultivated high yielding varieties HD-2967 and WH-1105 posing serious threat to wheat production in India[10].

Losses to wheat production due to yellow rust has been kept under control by breeding varieties having resistance genes. More than 50 yellow rust resistance genes (*Yr*) have been reported and deployed in wheat varieties to counter the pathogen[3]. In India, losses by yellow rust have been prevented by tactical deployment of these resistance genes, in addition due to excellent disease monitoring and containment during critical phases of crop has averted any epidemic in recent past. However, recently due to emergence of new virulent pathotypes, threat due to this disease has become an important concern both in India and world.

Mutation breeding for yellow rust resistance

Developing wheat lines with resistance to new virulent pathotypes is of utmost importance for national food security. However, developing wheat lines for disease resistance using conventional recombination breeding may take significant time and in cases where no genetic pool is available for resistance, it may become very cumbersome. Historically, disease resistance has been achieved using mutation breeding; it complements conventional breeding, with an advantage of resistance being achieved within the well adapted, accepted and high yielding genetic architecture of existing varieties.

A high yielding wheat variety, DBW-88 (released in 2014) was mutagenized by gamma rays at three different doses (viz. 250, 300 & 350 Gy), and M1 population containing ~ 3000 M1 plants was raised at Trombay during rabi season in 2015-16. Individual single plant harvests were advanced to M2 generation as plant- to- row progenies at ICAR-Indian Institute of Wheat and Barley Research (IIWBR), Karnal, which is a hot spot for yellow rust during rabi 2016-17. The M2 population having around 50,000 plants was screened for resistance to yellow rust under artificial epiphytotics with prevalent virulent races of NWPZ and nearly 100 putative variants showing resistance compared to parent were selected. To confirm the resistance in mutant progeny and further diversify the screening with other yellow rust races, putative mutant lines (M3) were advanced (ear to row) at IIWBR Karnal, summer nursery facility at Dalang Maidan (HP) in offseason 2016. 72 mutant lines showing enhanced resistance compared to parent DBW-88 were advanced (ear to row) in M4 generation during *rabi* 2016-17 and in the M5 during off-season, 2017. The selected 50 lines were evaluated during rabi 2017-18, the parent variety was susceptible (60-80S) and the mutants were immune (Fig. 2). These true breeding stable

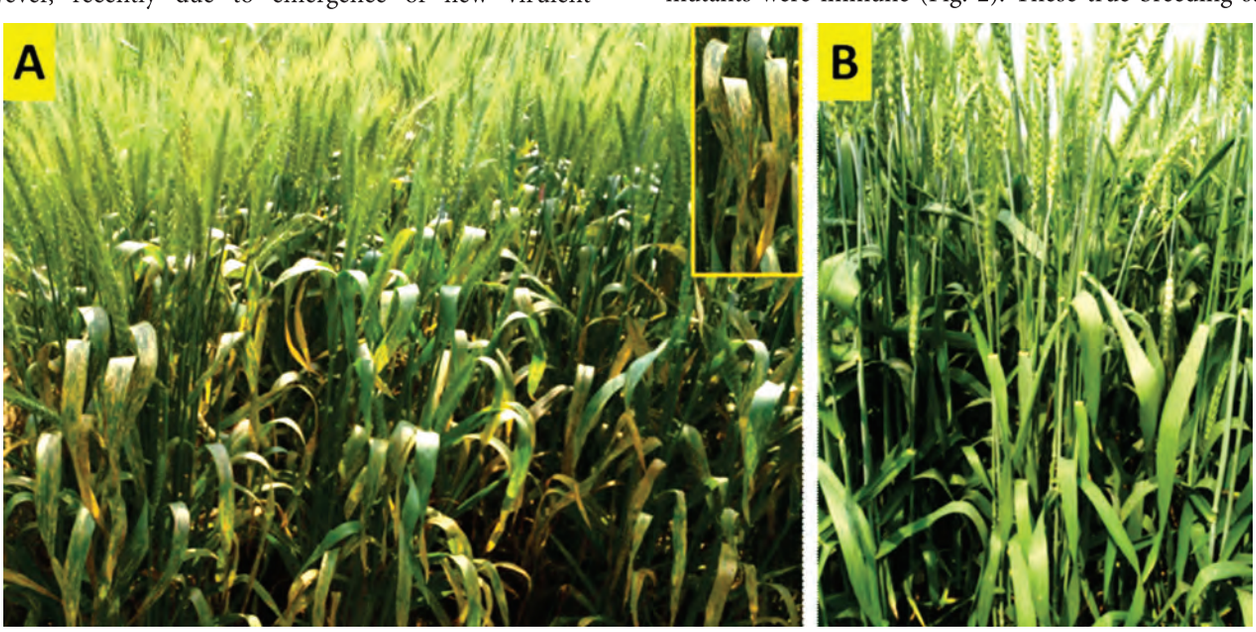

Fig. 2: Field reaction to wheat yellow rust at Karnal during *rabi* 2017-18 -A: Susceptible type response (60-80S) of parent variety DBW-88 (inset close view of susceptible reaction), (B): Immune type response of mutant lines

mutant lines will be evaluated for yield and other agronomic traits in upcoming winter season (2018-19). Further seedling resistance test, adult plant resistance test and gene postulation studies will be carried out to understand the nature of resistance in the mutant lines. The mutant lines provide excellent genetic resource for direct use against yellow rust and in addition as an indirect genetic variability to be used in recombination breeding. The mutants also provide pivotal models for studying molecular mechanism of resistance to stripe rust, which currently is not very well understood.

Conclusion and future scope:

Mutation breeding can be utilized to improve resistance in existing high yielding and popular wheat varieties without altering favourable combination of genes responsible for yield related traits. The current success in achieving resistance to yellow rust in DBW-88 has shown that, such an approach can provide solution to emerging races of yellow rust. Further to broaden genetic base for resistance to yellow rust, two other widely cultivated wheat varieties HD-2967 and WH-1105 were mutagenized and M2 was screened at IIWBR Karnal, putative mutants showing resistance to virulent races have been identified and will be confirmed in the upcoming season. In conclusion collaborative efforts between BARC and ICAR-IIWBR Karnal has led to development of useful mutants, which are excellent resources for improvement of wheat rust resistance and also its molecular understanding.

Acknowledgement

The authors are thankful to Associate Director (A) BSG, and Head, NA &BTD, BARC for kind support for carrying out the above work. The authors also thankful to Director, ICAR-IIWBR, Karnal for supporting mutation breeding research and providing research facilities.

References

1. Roberto J. Peña-Bautista, Nayeli Hernandez-Espinosa, Julie M. Jones, Carlos Guzmán,1 and Hans J. Braun. "CIMMYT Series on Carbohydrates, Wheat-Based Foods: Their Global and Regional Importance in the Food Supply, Nutrition, and Health". Cereal Foods World, 62(5), (2017): 231-249.
2. Alan P. Roelfs, Singh RP and Saari EE. Rust Diseases of Wheat: Concepts and Methods of Disease Management. Mexico, CIMMYT, 1992.
3. Robert A. McIntosh, Wellings CR and Park RF. Wheat rusts: an atlas of resistance genes. CSIRO Publishing, 1995.
4. David P. Hodson. "Shifting boundaries: challenges for rust monitoring". Euphytica,179 (2011): 93–104.
5. Tang Chunlei, Xiaojie W, Yulin Cheng ML, Liu M, Zhao M, Wei J and Kang Z. "New insights in the battle between wheat and Puccinia striiformis". Front Agric Sci Eng 2, (2015):101–114.
6. MS Hovmøller, Yahyaoui AH, Milus EA and Justesen AF. "Rapid global spread of two aggressive strains of a wheat rust fungus". Mol Ecol 17, (2008):3818–3826.
7. MS Hovmøller, Sørensen CK, Walter S and Justesen AF. "Diversity of Puccinia striiformis on cereals and grasses". Annu Rev Phytopathol 49, (2011):197–217.
8. S Nagarajan, Bahadur P and Nayar SK. "Occurrence of new virulence 47S102 of Puccinia striiformis West in India during crop Year 1982". Cereal Rusts Bulletin, 27, (1984): 28–31.
9. Mohinder Prashar, Bhardwaj SC, Jain SK and Datta D. "Pathotypic evolution in Puccinia striiformis in India during 1995–2004". Aust J Agric Res, 58, (2007):602–604.
10. Om P. Gangwar, Kumar S, Prasad P, Bharadwaj SC, Khan H, Verma H. "Virulence pattern and emergence of new pathotypes in Puccinia striiformis f. sp. tritici during 2011-15 in India". Indian Phytopathol, 69, (2016):178–185.

Report on the 3rd DAE-BRNS National Symposium on "Advances in Reactor Physics (ARP-2017) Fission Reactors – Now and Beyond

The 3rd DAE-BRNS national symposium on "Advances in Reactor Physics: Fission Reactors – Now and Beyond (ARP-2017)" was held at the DAE Convention Centre, Anushakti Nagar, Mumbai from December 6 - 9, 2017. This ARP symposium follows two such meetings arranged in the past, i.e. ARP-2007 with emphasis on 'Design, Analysis and Operation of Nuclear Reactors' and ARP-2013 on 'Simulation Techniques and Analysis Methodologies'. It is seventy five years since the first reactor Chicago Pile -1 went critical and the symposium also celebrated the Diamond Anniversary of first controlled chain reaction.

The 4-day symposium was organized by the Reactor Physics Design Division (RPDD) and was supported by Board of Research in Nuclear Sciences (BRNS) and Atomic Energy Regulatory Board (AERB). The symposium was inaugurated by Dr. R. Chidambaram, Principal Scientific Adviser to the Government of India who also delivered the inaugural lecture on current and future excitements in reactor physics research and development. In the inaugural function, the guests of honour Shri S. A. Bhardwaj, Chairman, Atomic Energy Regulatory Board; Shri S. K. Sharma, Chairman & Managing Director, NPCIL and Dr. D. N. Badodkar, Director, RD&DG, BARC, also addressed the participants. They all emphasised the importance and role of reactor physics in nuclear, fuel cycle and other related applications. Dr. Chidambaram also released the proceedings of the 3rd ARP symposium in book form as well as on CDROM.

The symposium attracted 150 delegates with participation from BARC, IGCAR, AERB, NPCIL including plant sites, BHAVINI, HBNI and a few from Indian universities. There were 6 participants from abroad. The deliberations were divided in 10 technical sessions spanned over 4 days, which included a Special Session commemorating 75th year of first reactor CP-1. This special session opened with a keynote address by Dr. Anil Kakodkar, AEC followed by three special lectures on energy from Fission, Fusion and Accelerator Driven Systems. Each of the technical sessions, opened with an invited talks followed by technical talks on specific areas of reactor physics and related fields, There were a 10 invited lectures from leading scientists including 6 foreign invitees. The symposium received overwhelming response from all over the DAE in form of 113 contributory papers which were reviewed by a panel of experts. Five of the contributory papers were selected for oral presentations and rest were presented in 2 poster sessions. Five contributory papers were awarded the best poster prizes. There were two evening talks, one by Dr. Shashank Chaturvedi, Director, IPR, Gandhinagar on "Energy from fusion – An overview" and another by Dr. K.P.N. Murthy, Chennai Mathematical Institute, Chennai on "Boltzmann - Microscopic Reversibility and Macroscopic Irreversibility".

The deliberations were involved and the meeting helped to gauge and assess the overall advancements in DAE (BARC, IGCAR and NPCIL).The symposium's technical program covered almost all the reactor types and topics pertaining to reactor design, safety, operation and energy systems for the future. These included Physics of existing NPPs, Advanced thermal reactor systems, Fast reactor physics, Innovative reactor concepts, Research Reactors, Nuclear data physics, Experimental Reactor Physics, Operational physics aspects of reactors, Advances in reactor analysis methods, Reactor fuel management, Fuel cycle physics, Reactor kinetics, Safety Studies and Safety analysis, Uncertainty and sensitivity studies, Multi-physics and multi-scale phenomena, Regulatory aspects, development of analysis tools, improvements in simulation techniques etc. The delegates from foreign countries: UK, Sweden, Japan, Korea and IAEA, spoke on the state-of-the-art on topics such as Nuclear Data,

Released the proceedings of the 3rd ARP symposium on CDROM

Core monitoring, Reactor noise, Spent Fuel Reactor, Thorium utilisation and alternative energy sources.

The concluding session of the ARP-2017 was held on 9th December, 2017. Dr. H.P. Gupta, Ex-RRF, BARC, summarised on the "Future Directions in Reactor Physics". The symposium concluded with a panel discussion chaired by Shri S. A. Bharadwaj, Chairman, AERB on the way ahead for physics of reactors. The delegates participated actively and had fruitful scientific interactions. It was recommended to assimilate the analysis capabilities of the various codes developed in DAE with emphasis on qualification, detailed documentation and benchmarking and to have validated nuclear physics data nuclear data libraries for different reactor spectrums.

DAE-BRNS Symposium on Nuclear Physics-2017

The 62nd DAE - BRNS Symposium on Nuclear Physics was held at Thapar Institute of Engineering and Technology (TIET) , Patiala, during December 19-24, 2017. The primary purposes of this series of symposia are (i) to discuss the research work done in these fields in India and abroad ; (ii) to enhance collaborative activities in the field of Nuclear Physics between R&D units of DAE and Universities; and (iii) to contribute to human resource development activity. Concepts and techniques of nuclear physics have evolved through a great deal of experimental and theoretical research. To give the participants a flavour of state of the art in the still thriving field, Invited Talks by experts from leading laboratories of the world were presented. Contributory papers were also presented which were selected after peer review from submissions from various centres of research in India; from DAE as well as university systems. One of the outcomes of the discussions held is an enhanced collaborative activity. It is heartening to see an increasing number of research scholars attending the symposia from year to year. This year, over 200 research scholars attended the symposium and the total number of participants was over 400 including a few from abroad. One of the main themes of the Symposium was Super Heavy Element Research. A pre-symposium orientation programme on this topic was held on 19th Dec. 2017 for the benefit of beginners .

A formal Inaugural Function was held on 20th Dec. 2017 which was presided by Prof. Prakash Gopalan, Director,TIET. The Inaugural Address was given by Prof. R. G. Pillay, Senior Professor, TIFR and the Keynote address was given by Prof. Amit Roy, Former Director- IUAC, New Delhi. Dr. A. Saxena, Head, Nuclear Physics Division, BARC, and Chairman, National Organising Committee, welcomed the delegates of the symposium and Dr. Bency John, Nuclear Physics Division, BARC, and Convener, National Organising Committee, gave an introduction to this year's symposium. Dr. N. K. Sahoo, Associate Director, Physics Group, BARC and Prof. O.P.Pandey, Dean of Research, TIET, also addressed the audience. Prof. Manoj K. Sharma, Convener, Local Organising Committee, and Dr. V. Jha, Secretary, National Organising Committee, proposed the vote of thanks during the inaugural and the concluding sessions of the symposium, respectively.

There was a special evening talk given by a distinguished speaker, Prof. R. Rajaraman, JNU, New Delhi, on the subject "Pauli Principle in the Interior of Pulsars and Fundamental Issues of Elementarity". There was a special session to select ' Prof. C. V. K. Baba Best Thesis Presentation Award instituted by Indian Physics Association and Dr. F. Zaidi of Aligarh Muslim University won the Award for her thesis titled "Nuclear medium effects in electromagnetic and weak structure functions at moderate Q^2". In addition, ten Best Poster Presentation Awards instituted by the National Organising Committee were presented during the Concluding Session of the Symposium held on 24th Dec. 2017. Dr. D. C. Biswas, Nuclear Physics Division, BARC, summarised all the scientific presentations of the symposium in the Concluding Session.

62nd DAE Solid State Physics Symposium 2017

The annual DAE - Solid State Physics Symposium (DAE SSPS 2017) was held at the DAE Convention Centre, Anushaktinagar, Mumbai, during December 26-30, 2017. This symposium is fully sponsored by Board of Research in Nuclear Sciences (BRNS), Department of Atomic Energy (DAE) and is held annually at different venues with a broad aim to bring together researchers working in various aspects of Condensed Matter Physics. About 1000 scientists, mostly from India and a few from abroad, participated in this symposium, which was 62nd in the series. Prof. Amitabh Das, Solid State Physics Division, BARC, and Convener, DAE-SSPS 2017, welcomed the delegates of the symposium and gave an introduction to the symposium, in the inaugural session. The symposium was inaugurated by Prof. N.K. Sahoo, Assoc. Director, Physics Group, BARC. Prof. P.R. Vasudeva Rao, Vice Chancellor, HBNI and Dr. A. K. Sinha, Director, UGC-DAE Consortium for Scientific Research, Indore, in their address as chief guests of the symposium highlighted the importance of solid state physics research. Dr. D. Bhattacharyya, Chairman, Local Organising Committee addressed the delegates. Dr. Surendra Singh, Scientific Secretary, 62nd DAE-SSPS 2017, proposed the vote of thanks.

Inaugural Session of the 62nd DAE SSPS 2017: Standing on the dais from right to left are: Dr. Amitabh Das (Convener), Prof. N. K. Sahoo (AD, Physics Group, BARC), Prof. P R Vasudeva Rao (VC, HBNI, Mumbai), Prof. A. K. Sinha (Director, UGC-DAE Consortium for Scientific Research, Indore) Dr. D. Bhattacharyya (Chairman, Local Organising Committee), Dr. Surendra Singh (Scientific Secretary)

The technical session of this symposium was divided into invited talks, contributory papers in the form of oral and poster presentations, presentations by Ph.D. thesis candidates and Young Achiever Award (YAA) nominees. This year, there have been very enthusiastic responses in terms of the number of papers submitted. We had received 1402 contributory papers from which 840 papers were chosen for presentation after a due review process by experts. In this symposium, 2 plenary talks, 49 invited talks, 24 oral presentations, and 800 posters were presented. The topics covered in the symposium were (a) Phase transitions (b) Soft Condensed Matter including Biological Systems (c) Nano-materials (d) Experimental Techniques and Devices (e) Glasses and Amorphous Systems (f) Surfaces, Interfaces and Thin Films (g) Electronic Structures and Phonons (h) Single Crystals and Characterization (I) Transport Properties (J) Semionductor Physics (K) Superconductivity, Magnetism and Spintronics (l) Energy Materials. There were 8 thematic seminars on (i) Energy Materials (ii) Superconductivity (iii) Applied Physics (iv) Nanomaterials (v) Condensed Matter-Theory (vi) Science using Neutron and Synchrotron facilities (vii) Functional / Nanomaterials (viii) Soft Condensed Matter.

Two outstanding plenary talks were delivered on Organic-inorganic hybrid ferroelectric perovskite materials for photovoltaic applications: The role of the polar field and other related issues by Prof. D. D. Sarma, Indian Institute of Science, Bangalore, and Discovery of superconductivity of very pure single crystal of Bismuth by Prof. S. Ramakrishnan, Tata Institute of Fundamental Research, Mumbai. The evening talks were delivered by Prof. G. K. Dey, Former Director, Material Group, BARC, Mumbai on Viewing biological and non-biological matter through the Transmission Electron Microscope and by Prof. S. P. Kale, Former Associate Director, Bioscience Group, BARC on Enviro - Economics of Our Life.

A panel of judges selected 3 Young achiever awards out of 9 participants. Another Panel of judges selected 3 best Ph.D. thesis awards out of 30 participants. Another panel of judges selected 24 best poster awards out of 800 posters. In the concluding session, YAA awards and Ph. D. thesis award were given away by Prof. N. K. Sahoo (Assoc. Director, Physics Group, BARC) and Prof. S. M. Yusuf (Head, Solid State Physics Division, BARC). The best poster awards were distributed by Prof. Vaishali Bambole (Head Physics Department, University of Mumbai), Prof. M. Senthil Kumar (IITB, Mumbai), and Prof. P. K. Mandal (Univ. North Bengal, Siliguri, WB). The best thesis award presented to Ms. Nasrin Banu titled "Structure, Magnetic Properties and their Ion Irradiation Induced Modifications in Thin Films and Multilayers" was sponsored by the Indian Physics Association (IPA) as IPA's Anil K. and Bharati Bhatnagar Best Ph.D. Thesis Award in Solid State Physics.

Release of the Founder's Day Special Issue of the BARC Newsletter

Founder's Day special issue of the BARC Newsletter was released by Director, BARC on 30th October, 2017 carrying 24 Award winning Papers, out of which 3 were from Homi Bhabha Science & Technology Awardees, 10 from Scientific & Technical Excellence Awardees, 6 from Young Applied Scientist / Technologist Awardees, 4 from Young Scientist Awardees, 1 from Young Engineer Awardee.

DAE (Excellence in Science, Engineering & Technology) Award 2016

A. Homi Bhabha Science & Technology Awardees

1. Shri R. B. Bhatt, SO/H+, A3F, NRB, BARC

Shri R. B. Bhatt has been awarded for his innovative research contributions in field of "MOX fuel fabrication". He has designed, developed and commissioned a new MOX fuel fabrication line and fabricated the fuel elements for the first core of the Prototype Fast Breeder Reactor. He pioneered the use of lasers in fuel fabrication and introduced techniques such as laser welding in place of traditional TIG welding and laser decontamination instead of ultrasonic decontamination of fuel pins.

2. Dr. A. K. Arya, SO/H+, MMD, MG, BARC

Dr. A.K. Arya has been awarded for his innovative research contributions in field of "Alloy Phase Stability & Phase Transformations, Materials Modeling and Quantum and statistical mechanical simulations of materials". He has made a major contribution to the development of computational tools for materials modeling and design. He has generated a database of thermo-physical properties of thoria-based mixed oxide fuels to understand their behaviour during irradiation and under accidental conditions.

3. Shri U. D. Malshe, SO/H+, ED&DD, MRG, BARC

Shri U.D. Malshe has been awarded for his innovative research contributions in field of "Design and development of mechanical components". He has made contribution in the field of studies related to nuclear power growth and developing facilities as well as mechanical systems associated with nuclear fuel materials. His contributions in developing software tool HEEP has made a good international impact by providing a unique and versatile tool to estimate cost of hydrogen production to assess its economy.

4. Shri R. Keswani, SO/H, MFD, NFG, BARC

Shri R. Keswani has been awarded for his innovative research contributions in field of "Handling processing and storage of nuclear materials". He developed expertise in handling, processing, transportation and storage of special alloy components and systems. Alloy fabrication program has registered impressive growth in annual throughputs consistently, with record outputs in recent times.

5. Dr. S. Gautam, SO/G, FTD, BSG, BARC

Dr. S. Gautam has been awarded for his innovative research contributions in field of "Food Technology". He has developed several technologies to address post-harvest losses of exotic and ethnic fruits such as mango, litchi, pomegranate, grapes, apple, banana, pineapple and papaya using radiation or chemical treatment to extend their shelf-life and enable cost-effective transportation within India and for export. Dr. Gautam conceptualized a design of a treatment plant which led to the development of a 1 ton per hour litchi treatment machine.

6. Dr. S. Santra, SO/H, NPD, PG, BARC

Dr. S. Santra has been awarded for his innovative research contributions in field of "Experimental Nuclear Physics ". He has successfully implemented many new ideas in heavy ion reaction studies using FOlded Tandem Ion Accelerator FOTIA and Pelletron Accelerator. Has investigated the effect of projectile breakup on fusion, elastic scattering and fission for many reactions, leading to a systematic understanding of the role of projectile breakup threshold and target atomic number on these reactions.

7. Shri S. K. Bose , OS, CD, E&IG, BARC

Shri S.K. Bose has been awarded for his innovative research contributions in field of "Computer Graphics, Computer Vision and High Performance Computing". He has developed A 3D stereoscopic visualization system for microscopy and deployed in AIIMS, New Delhi for Neurosurgery Training. He has Developed a tiled display for high resolution images and movies using parallel processing techniques and computer graphics and augmented reality assisted telerobotics system for autonomous pick and place operation from stereo image.

8. Dr. D. Mandal, SO/H, AMMD, ChEG, BARC

Dr. D. Mandal has been Awarded for his innovative research contributions in field of "Chemical Engineering". He has Developed the 'Solid State Reaction Process' to synthesize and fabricate lithium-titanate pebbles, which find utility as solid breeder material for the Test Blanket Module in fusion reactors. He had taken the development from lab scale to the stage of large scale continuous production process.

B. Exceptional Service Awardee

1. Dr. G. J. Prasad, Former Director, NFG, BARC

He has Awarded for his excellent contributions in the field of "Development and fabrications of Nuclear fuels". Under his inspired and able leadership, the teams engaged in the fuel fabrication efforts have accomplished challenging targets within stringent time frame with due regard to all safety aspects.

Central Complex at BARC

Edited & Published by:
Scientific Information Resource Division
Bhabha Atomic Research Centre, Trombay, Mumbai 400 085, India
BARC Newsletter is also available at URL:http://www.barc.gov.in